THEORY

JET FIRE

DATE: December 2023

This document describes the theory of the single and two-phase Jet Fire (JFSH) model which is implemented in PHAST and SAFETI. The validation of the JFSH and radiation (RADS) models against field data is published in the companion validation document. The jet flame is modelled either as a conical frustum emitting radiation from its surface with uniform surface emissive power or as a distribution of individual point sources along the flame centreline (multi-point source emitter). The conical frustum model predicts the flame and frustum lengths, frustum base and tip widths, angle between the frustum and release axes, lift-off distance of the frustum from the release plane, fraction of heat radiated from the flame's surface, and maximum surface emissive power of the flame. The multi-point source model predicts flame characteristics as in the conical model except, frustum base and tip widths, and maximum surface emissive power. Radiation emitted along the flame centreline is modelled in terms of a weighting factor representing the proportion of combustion energy multiplied by a fixed fraction of heat radiated at different positions along the flame length.

No.	Date	Reason for Issue	Prepared by	Verified by
1	May 2004	Jet Fire Improvement Project	A. O. Oke	H. Witlox and D. Worthington
2	July 2004	PHAST/SAFETI 6.5 Jet Fire Model Upgrade Project	A. O. Oke	D. Worthington
3	March 2011	Upgraded for 6.70	Y. Xu	H. Witlox
4	April 2012	Extended 2-phase 6.7 validation with Eelke Kooi (RIVM)	H. Witlox	
5	August 2015	Further extended validation; rotate fire if hits ground	Y. Xu and H. Witlox	H. Witlox
6	December 2020	Modifications for 8.4 - time varying releases and stoichiometry	David Worthington	A. O. Oke, J. Pickles
7	May 2021	Apply new template	D. Vatier	
8	October 2021	Updates for 8.6 – Miller (2017) model extensions, removal of validation to a companion validation document	A.O. Oke	Y. Xu, D. Worthington and J. Stene

Date: December 2023

Prepared by: Digital Solutions at DNV

ABSTRACT

This document describes the theory of the single and two-phase Jet Fire (JFSH) model which is implemented in PHAST and SAFETI. The companion validation document compares predictions of the JFSH and radiation (RADS) models against field data. Two types of jet fire models are described: cone-shaped flame models and a line source emitter flame model.

In cone-shaped flame models, the jet flame is modelled as a conical frustum, emitting radiation as a solid body with uniform surface emissive power. The models predict the flame and frustum lengths, frustum base and tip widths, angle between the frustum and release axes, lift-off distance of the frustum from the release plane, fraction of heat radiated from the flame's surface, and maximum surface emissive power of the flame.

Three conical frustum jet flame models are presented. These are: JFSH-Chamberlain, based on the Shell pure-vapour model by Chamberlain; JFSH-Cook, based on the modified jet flame correlations proposed by Cook et al. (1990) to account for vapour and especially liquid and two-phase releases and JFSH-Johnson, which is an improvement to the JFSH-Chamberlain model to account for horizontal/near horizontal vapour phase releases. The dimensions of the conical frustum, and its orientation in space, as employed in the JFSH-Chamberlain and JFSH-Johnson model, were correlated semi-empirically from results of laboratory and field studies. The Chamberlain, Cook and Johnson models account for the influence of wind speed, air entrainment rate and crosswind effects on flame characteristics.

The multi-point source emitter flame model, Miller model, is based on AP flame (Miller, 2017). The Miller model is an extension of the Chamberlain model, particularly to low luminosity gases, such as hydrogen (Miller, 2017). The jet fire is modelled as a distribution of individual point sources along the flame centreline. The Miller model predicts flame characteristics as in the Chamberlain model except, frustum base and tip widths, and maximum surface emissive power. Radiation emitted along the flame centreline is modelled in terms of a weighting factor representing the proportion of combustion energy multiplied by a fixed fraction of heat radiated at different positions along the flame length.

The JFSH-Cook, JFSH-Chamberlain, JFSH-Johnson and Miller multi-point source (M-MPS) models have been validated by comparing their predictions with appropriate field data reported by Chamberlain, Bennett et al., Miller, Selby and Burgan. Within limits of uncertainty, predictions from the JFSH-Cook and JFSH-Chamberlain models for pure vapour jet flames resulting from vertical releases show good agreement with field data with a maximum absolute deviation and mean deviation of 12.5% and 5.0% respectively when compared with predictions from the Chamberlain model. Based on available field data for horizontal liquid/two-phase releases, the JFSH-Cook liquid/two-phase jet fire model generally predicts flame lengths to within ±30% of measurements, while average estimates of flame SEP lies within -30% of measured data. For horizontal vapour phase releases, the JFSH-Johnson model predicts flame lengths to within ±10% of available field data.

The simulation of received radiation by objects at a distance from a jet flame, using the RADS model, has been validated against field data gathered by Chamberlain and Bennett et al for vertical and horizontal jet flames respectively. Simulated results were based on flame characteristics predicted by the JFSH-Cook, JFSH-Chamberlain and JFSH-Johnson models. The predicted incident radiation over a wide range of observer locations and orientations compare well with field data and generally lie within ±40% of measurements.

The comparison of each model including the data set used by Miller to develop his model is explained in the companion validation document. The results have enabled some advice as to which model to use for different types of release;

- The Cook model for non-vapour releases
- The Miller model for low luminosity gases (e.g. hydrogen and syngas)
- The Chamberlain model for all other releases except horizontal vapour releases where the Johnson model is recommended.

Table of contents

ABSTRACT I

1 INTRODUCTION 4

2 THE VAPOUR PHASE JET FIRE MODEL 5
2.1 Calculation of the post-expansion jet velocity (v_j) or expanded radius (r_j) 9
2.2 Calculation of the effective source diameter (D_s) 9
2.3 Calculation of the Flame length (L_B) 9
2.4 Calculation of angle between hole and flame axes (α) 11
2.5 Frustum lift off 12
2.6 Calculation of the frustum length (R_L) 12
2.7 Calculation of width of frustum base (W_1) 12
2.8 Calculation of width of frustum tip (W_2) 13
2.9 Surface emissive power ($W_{surface}$) 13
2.10 The flame co-ordinates 14
2.11 Determination of likelihood of flame touch down or on-ground impingement 16

3 THE LIQUID/TWO-PHASE JET FIRE MODEL 16
3.1 Effective Source Diameter 16
3.2 Mass discharge rate – two phase releases 17

4 THE MILLER (M-MPS) JET FIRE MODEL FOR LOW-LUMINOSITY GASES 17
4.1 Introduction 17
4.2 Calculation of wind speed at flare tip (U_w) 20
4.3 Calculation of still air flame length parameters for non-hydrocarbons 20
4.4 Angle between flame axis (flame tilt or lift) and the horizontal, α_{AP} 21
4.5 Calculation of flame momentum (B_M) and lift-off (B) distances 22
4.6 Flame centreline (L_f), hole-to-tip (L_B) and frustum (R_L) lengths 22
4.7 Calculation of radiant heat fraction and radiation characteristics 23
4.8 Calculation of equivalent natural gas flowrate using similarity approach 24
4.9 Modelling of crosswind impact for non-vertical releases 24
4.10 Modelling of radiation impact on planar observers 25
4.11 Application of numerical integrators for radiation effect modelling 25
4.12 Finite flame lift-off distance and height relative to release location 27
4.13 Application of the HyRAM radiative fraction correlation 27
4.14 The flame (centreline) co-ordinates 28

5 ADJUSTMENT OF JET FIRE FOR TIME VARYING RELEASES 28
5.1 Options available 28
5.2 Fireball matching method 29

6 ADJUSTMENT OF FLAME SHAPE IN CASE OF GROUND IMPINGEMENT 29

7 FUTURE DEVELOPMENTS 32

NOMENCLATURE 33

REFERENCES 36

Table of figures

Figure 1 Jet-fire geometry (Chamberlain model accounting for crosswind effects)..... 6
Figure 2 Jet-fire geometry (side view) ignoring crosswind effects (JFSH-Cook model)..... 7
Figure 3 Jet-fire for horizontal jet fire model (Johnson et al.)..... 8
Figure 4 Miller model flame representation for horizontal jet fires.....18
Figure 5 Miller model flame representation for vertical jet fires.....18
Figure 6 Miller model radiation intensity distribution 19
Figure 7 Flame adjustment for flame penetrating the ground 30
Figure 8 Determining the adjusted flame position.....31

List of tables

Table 1 Methods for calculating average rates and impact on jet fire modelling.....28

1 INTRODUCTION

A jet flame occurs following the ignition and combustion of a flammable fluid issuing continuously from a pipe or orifice, which burns close to its release plane. Releases that fuel jet fires could be accidental or intentional. An example of the latter are jet flames from flare systems of offshore oil and gas production facilities, which are primarily operated to provide a safe means of disposal of hydrocarbon gas under a variety of process conditions. Jet flames dissipate thermal radiation, which, away from the flame's visible boundaries, transmit heat energy that could be hazardous to life and property. Thus, in the evaluation of the hazard posed by jet flames, the accurate determination of the likelihood of flame impingement and/or the amount of radiant energy received by objects at a distance from the flame is of primary importance.

Model Categories

Models developed for estimating the received radiated heat flux by objects at a distance from jet flames can be divided broadly into three categories[1]. These are: Semi-empirical, Field, and Integral models.

Semi-empirical models are relatively simple and are usually designed to predict quantities such as flame shape and heat fluxes to external objects without providing a detailed description of the fire itself. They can be further divided into: point source, multiple point source and surface emitter models. Point source models do not attempt any shape prediction and represent the source of heat radiation by a point (e.g., API-521 model[2]). On the other hand, multiple point source models attempt to model the effect of flame shape on radiated heat flux by representing the flame with a flame centreline trajectory along which several radiating point sources are distributed. Surface emitter models represent the flame by a solid object (usually a cone or a cylinder) from which heat is being radiated.

Field models are formulated on solutions of the time-averaged Navier-Stokes-equations for conservation of mass, momentum and other scalar quantities in a flowing fluid. Field models require additional sub-models in order to adequately describe important physical and chemical processes taking place during the combustion of a flowing fluid. They are mathematically complex, require a lot of effort in coding and expend significant run times on high performance computer systems.

Integral models are a compromise between semi-empirical and field models. In these models, with the aid of simplifying assumptions, the partial differential equations coupled with the sub-models in field models are reduced to ordinary differential equations and subsequently integrated. They are less rigorous and less computationally expensive when compared with Field models.

Of the three modelling categories described above, semi-empirical models are the most attractive with respect to hazard assessment purposes. In comparison with integral or field models, semi-empirical models are mathematically simpler, easier to understand and formulate, quicker to implement in computer programs, require significantly shorter computational run times, and predict flame properties that are of interest to hazard assessment studies with reasonable accuracy. However, semi-empirical models are heavily dependent on experimental data, and are limited to the specific type of fire studied during experimentation and the range of conditions under which model correlations were derived.

JFSH/M-MPS models

In all, a number of semi-empirical models exist for jet fire modelling that have been correlated over a wide range of conditions encompassing typical jet fires encountered in reality. Of these, the basic features of the surface emitter model by Chamberlain[3], which was later extended by Johnson et al. (1994)[4], as well as a further extension by Miller (2017)[5], i.e., the Miller multipoint source emitter flame model (M-MPS), have been adopted and implemented in the JFSH model.

The Chamberlain model was originally developed for modelling jet fires resulting from vertical/inclined (i.e. angle of inclination $\leqslant 45^{o}$ from the vertical) vapour phase releases[3]. The Johnson et al. model specifically simulates jet flames resulting from horizontal/near horizontal vapour phase releases. In the JFSH-Cook model, the Chamberlain model has been modified in order to account for changes in effluent buoyant behaviour following liquid or two-phase release. The Chamberlain model, when compared with point or multiple point source models, gives a better physical description of flame behaviour by its representation of a flame with a solid body (conical frustum) emitting radiation from its surface. The model's flame shape representation is more attractive as it removes many of the geometrical inadequacies of point-source models. In contrast to multiple point source (centreline trajectory) models, the Chamberlain model is easier to program, requires less computational effort (shorter run times), provides a similar level of accuracy in predictions, and supports an analytical resolution of its heat radiation calculations.

The Miller model was primarily developed for low to high pressure releases of non-hydrocarbon/low-luminosity gases, pointed downwind in the horizontal, vertical or 45^{o} inclined release directions. The jet flame is modelled as a distribution of individual point sources along the flame centreline. The model predicts flame characteristics as in the Chamberlain model except, frustum base and tip widths, and maximum surface emissive power. Radiation emitted along the flame centreline is modelled in terms of a weighting factor representing the proportion of combustion energy multiplied by a fixed fraction of heat radiated at different positions along the flame length.

The first step in estimating flame dimension and orientation involves the calculation of the discharge followed by the post-expansion state of the fluid at ambient pressure. During this calculation, the post-expansion fluid state (i.e., temperature or liquid fraction) plus the post-expansion fluid velocity or expanded radius are determined. Subsequently, the effective source diameter corresponding to the physical state of the fluid is estimated. The iterative calculation of flame length in still air follows, from which other parameters that describe the flame dimension and orientation in space are determined. Using an empirical correlation expressed as a function of the ratio of the wind speed and post-expansion velocity of the escaping fluid, the fraction of heat radiated from the flame is determined. The latter in conjunction with the heat of combustion of the released fluid is employed in estimating the surface emissive power of the flame. The correlation employed in the JFSH-Cook model for estimating the frustum base width differs from that presented in the Chamberlain model. For liquid or two-phase releases, the equations employed in the Chamberlain model for the effective source diameter and lift-off distance are slightly modified in the JFSH-Cook model to try to account for changes in the buoyant behaviour of the release.

Chapter 2 describes the vapour phase jet fire model, including the JFSH-Chamberlain, JFSH-Johnson and JFSH-Cook models. Chapter 3 describes the modifications applied in the JFSH-Cook model to model the jet flame from a liquid or two-phase release. Chapter 4 sets out the M-MPS flame model correlations and extensions to JFSH-Chamberlain/Johnson for low-luminosity/non-hydrocarbon flames. Chapters 5 and 6 describe the adjustment of the flame source term for time varying releases and flame shape in case of ground impingement, respectively. In Chapter 7, the document closes with suggestions on possible improvements to the JFSH jet fire models.

2 THE VAPOUR PHASE JET FIRE MODEL

Figure 1 shows the basic features of the conical frustum used in the Chamberlain model to describe a jet fire for all wind directions.

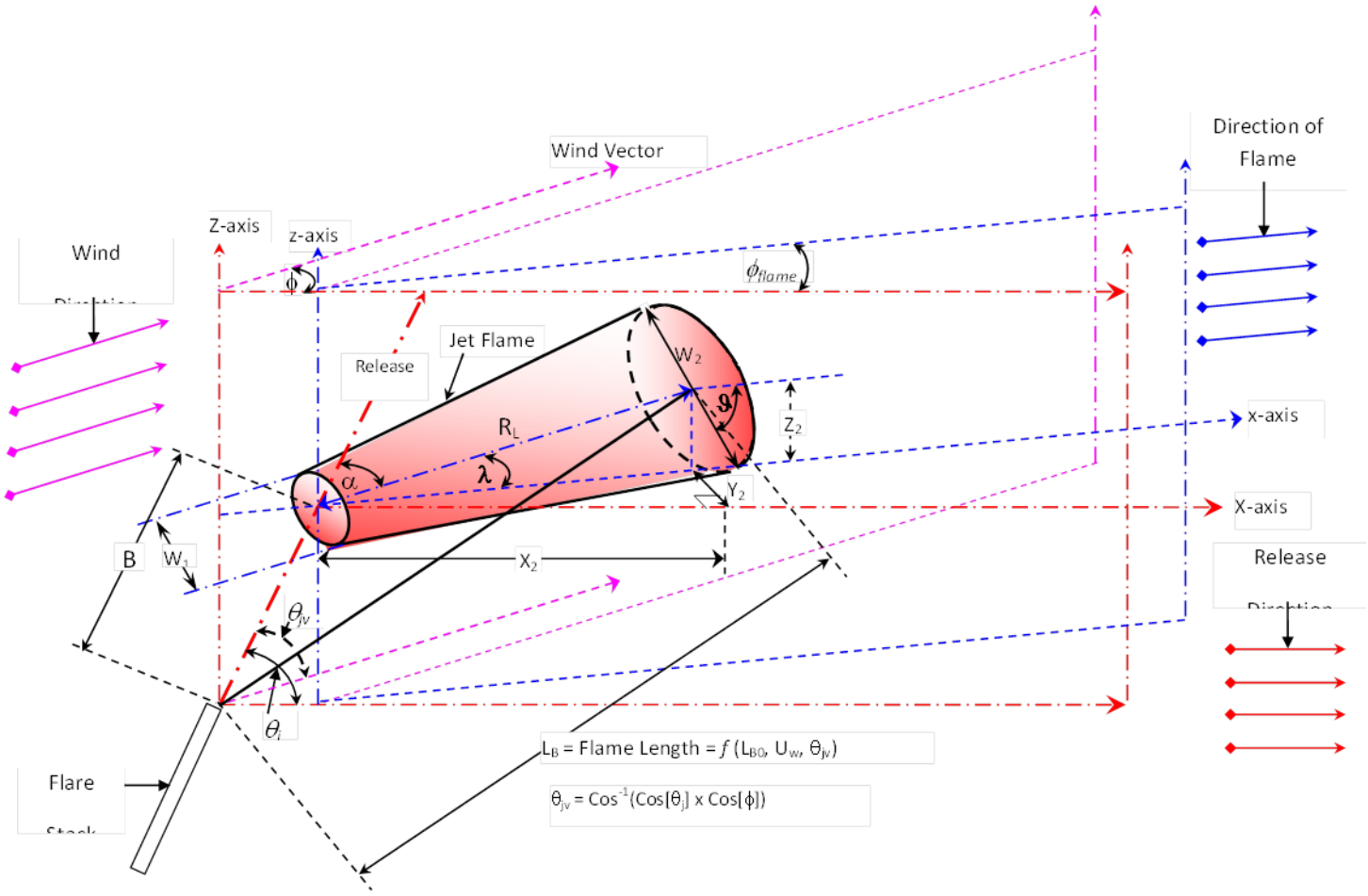

Figure 1 Jet-fire geometry (Chamberlain model accounting for crosswind effects)

Figure 2 on the other hand shows jet flame dimensions for the special case in which the prevailing wind and pipeline axis lie in the same direction (i.e., ignoring crosswind effects).

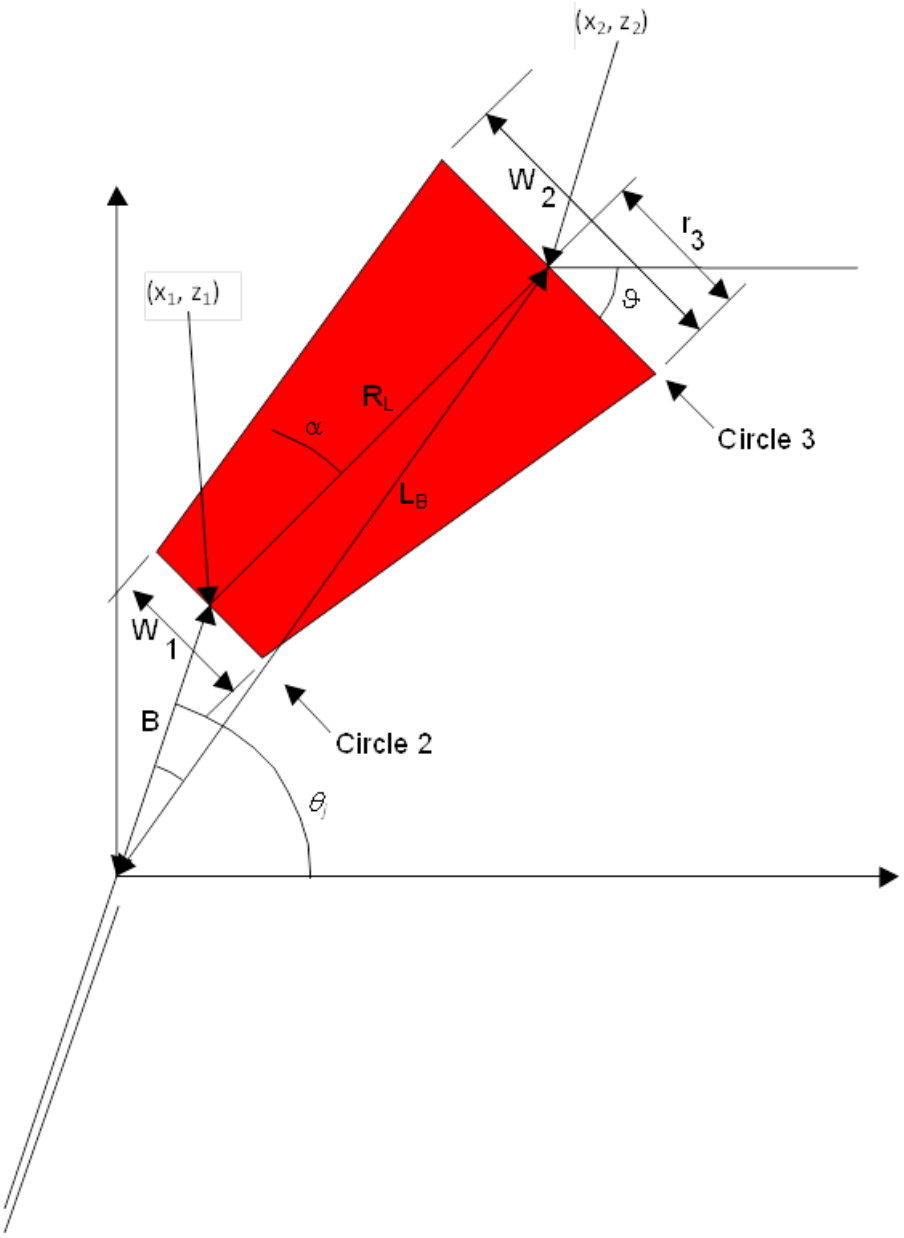

Figure 2 Jet-fire geometry (side view) ignoring crosswind effects (JFSH-Cook model)

Figure 3 is a schematic representation of the flame shape and dimensions as employed in the Johnson et al. (1994) model. Expressions describing the dimensions of the conical frustum and fraction of heat radiated from the flame under a wide range of ambient and flow conditions have been correlated from laboratory and field tests.

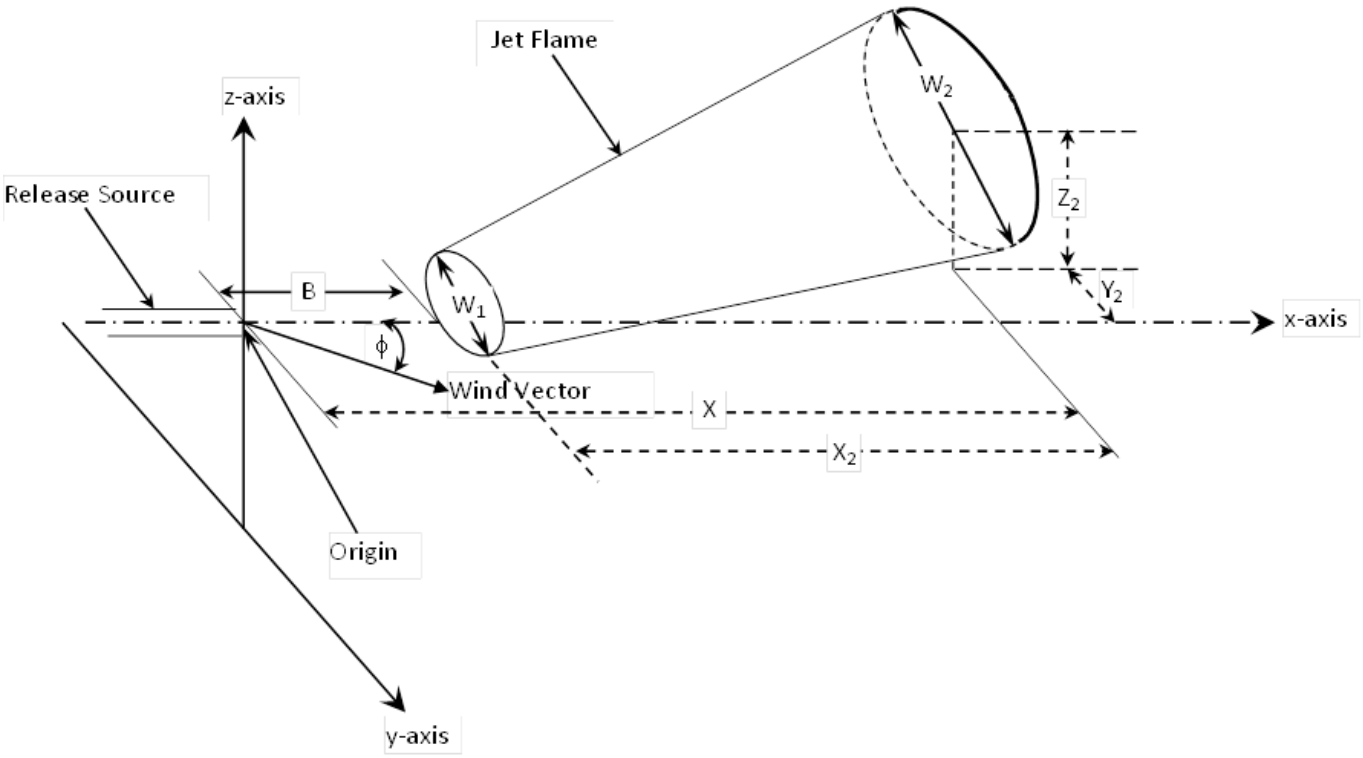

Figure 3 **Jet-fire for horizontal jet fire model (Johnson et al.)**

Prior to determining the flame dimensions, the model requires the determination of the post-expansion properties of the fluid. These correspond to the dynamic and thermodynamic states of the fluid following its expansion from storage conditions to ambient pressure. The thermodynamic state of the fluid is defined by either its post-expansion temperature (single-phase) or liquid mass fraction (two-phase), while the fluids' dynamic state is defined by either its expanded radius or post-expansion velocity. The DISC[6] model is employed in simulating the fluid expansion process from storage to discharge conditions. Subsequently, the DISC model invokes the ATEX[7] model to determine the post-expansion characteristics of the released fluid.

The flame orientation and dimensions followed by its surface emissive power are determined using a combination of empirical correlations and relationships derived from analytical plane geometry. The algorithm employed in determining the flame (frustum) dimensions and its surface emissive power based on the Chamberlain model is summarised below:

- Depending on input to the jet fire model, calculate either the post-expansion jet velocity (v_j) or expanded radius (r_j)
- Calculate the effective source diameter (D_s)
- Calculate the flame length (L_B)
- Calculate angle (α) between the hole axis and flame axis
- Calculate frustum lift off distance (B)
- Calculate frustum length (R_L)
- Calculate width of frustum base (W_1)
- Calculate width of frustum tip (W_2)
- Calculate the surface emissive power of the flame ($W_{surface}$)
- Determine the flame co-ordinates
- Determine the likelihood of flame touch down (ground impingement)

In the following, the equations employed in the JFSH-Cook, JFSH-Chamberlain and JFSH-Johnson models are presented.

2.1 Calculation of the post-expansion jet velocity (v_j) or expanded radius (r_j)

Depending upon the post-expansion dynamic state input supplied to the JFSH model, either the jet velocity or the expanded radius is calculated as:

Jet velocity

$$v_j = \frac{m}{\rho_j \pi r_j^2} = \frac{\text{Mass discharge rate } (\text{kg s}^{-1})}{(\text{Mass density } (\text{kg m}^{-3})) \times (\text{Cross-sectional area } (m^2))} \quad (1)$$

Expanded radius

$$r_j = \left(\frac{m}{\rho_j \pi v_j}\right)^{\frac{1}{2}} \quad (2)$$

Where:

ρ_j	=	Post-expansion density of the fluid [kg m^{-3}]
m	=	Mass discharge rate [kg/s]
v_j	=	Post-expansion velocity of the fluid [m/s]
r_j	=	Expanded radius of the escaped fluid [m]

2.2 Calculation of the effective source diameter (D_s)

The effective source diameter represents the throat diameter of an imaginary nozzle from which air at ambient density issues with the same mass flow rate and velocity as the fuel. For pure vapour release, the effective source diameter is given by [3]:

$$D_s = 2r_j \sqrt{\frac{\rho_j}{\rho_{amb}}} \quad (3)$$

Where:

ρ_{amb}	=	Ambient air density [kg/m^3]

2.3 Calculation of the Flame length (L_B)

For all wind speeds and directions, Chamberlain suggested the following expression for the calculation of flame length[3]:

$$L_B = L_{B0}\left(0.51e^{-0.4U_w} + 0.49\right)\left(1 - 0.00607\left(\theta_{jv} - 90\right)\right) \quad (4)$$

Where:

L_{B0}	=	Flame length in still air [m]
U_w	=	Wind speed [m/s]
θjv	=	Angle between release direction and wind vector in the plane containing the release direction, flame axis, and wind vector [o] (see Figure 1)

In the absence of crosswind effects, θ_{jv} in equation (4) is replaced by θ_j (see Figure 1)[8].

Where:

θ_j = Angle between hole axis and the horizontal in the vertical plane [o] (see Figure 1)

In the Johnson et al. model, the flame length from plane geometry is expressed as:

$$L_B = \sqrt{(X^2 + Y^2 + Z^2)} \quad (5)$$

Where X, Y and Z refer to the position of the centre of the frustum tip with respect to the flare tip (origin) (see Figure 3). From extensive experimental data, X, Y and Z have been correlated in terms of dimensionless numbers and are respectively given by[4]:

$$X/L_{B0} = f(\xi)(1 + r(\xi)\Omega_x) \quad (6)$$

$$Y/(X - B) = 0.178\Omega_y \quad (7)$$

$$Z/L_{B0} = h(\xi)(1 - c(\xi)\Omega_x) \quad (8)$$

Note: Equation (8) is subject to the following constraint[4]: $0.0 \leqslant Z/L_{B0} \leqslant 1.0$ while a similar constraint is imposed on equation (7) and is given by: $-1.0 \leqslant Y/L_{B0} \leqslant 1.0$

B is the luminous flame lift-off distance (described later, see section 2.5), while Ωx and Ωy are dimensionless parameters which represent the balance between the initial jet momentum flux and the wind momentum flux in the x and y directions respectively (see Figure 3). Ωx and Ω_y are given by[4]:

$$\Omega_x = \left[\frac{\rho_{amb}}{\rho_j}\right]^{1/2}\left[\frac{L_{B0}U_w \cos\varphi}{d_j v_j}\right] \quad (9)$$

$$\Omega_y = \left[\frac{\rho_{amb}}{\rho_j}\right]^{1/2}\left[\frac{L_{B0}U_w \sin\varphi}{d_j v_j}\right] \quad (10)$$

The variables $f(\xi)$, $r(\xi)$, $h(\xi)$, $c(\xi)$ are expressed respectively as[4]:

$$f(\xi) = \begin{cases} 0.55 + (1 - 0.55)e^{(-0.168\xi(L_{B0}))} & \xi(L_{B0}) \leq 5.11 \\ 0.55 + (1 - 0.55)e^{(-0.168\xi(L_{B0}) - 0.3(\xi(L_{B0}) - 5.11)^2)} & \xi(L_{B0}) > 5.11 \end{cases} \quad (11)$$

$$r(\xi) = \begin{cases} 0.0 & \xi(L_{B0}) \leq 3.3 \\ 0.082\left(1 - e^{(-0.5(\xi(L_{B0}) - 3.3))}\right) & \xi(L_{B0}) > 3.3 \end{cases} \quad (12)$$

$$h(\xi) = 1/(1 + 1/\xi(L_{B0}))^{8.78} \quad (13)$$

$$c(\xi) = 0.02\xi(L_{B0}) \quad (14)$$

Where:

$\xi(L_{B0})$ = Richardson number based on flame length in still air = $\left(\frac{g}{D_s^2 v_j^2}\right)^{\frac{1}{3}} L_{B0}$

In the calculation of the flame length, the only unknown in equations (4)-(14) is L_{B0}. It is obtained from the iterative solution of Kalghatgi's[9, 3] correlation derived from experiments on vertical flames in still air. The correlation is given by:

$$\left(\frac{D_s \beta}{L_{B0} W_{st}}\right)^{\frac{2}{3}} = 0.2 + 0.024\xi(L_{B0}) \quad (15)$$

Where:

β	=	Becker and Liang's[10], [3] flame length constant	=	$\left(\frac{W_{\mathrm{Air}}T_1}{W_pT_{\mathrm{Air}}}\right)^{\frac{1}{2}}$
W_{st}	=	Mass fraction of fuel in a stoichiometric mixture with air [-]		
g	=	Gravitational acceleration [m/s^2]		
W_p	=	Mean product molecular weight [kg/kmol]		
W_{Air}	=	Molecular weight of air [kg/kmol]		
T_1	=	Adiabatic combustion temperature [K]		
T_{Air}	=	Air/ambient temperature [K]		

For a paraffin of molecular weight (M_W), the stoichiometric mass fraction (W_{st}) of the fuel in air has been derived by Chamberlain as[3]:

$$\boldsymbol{W_{st} = \frac{M_W}{15.816\ M_W + 39.5}} \qquad \textbf{(16)}$$

However, equation (16) is only valid for paraffins and so in JFSH there is an option to calculate W_{st} calculated using the DIPPR property system. This allows the model to be extended to alternative fuels and mixtures

Assuming typical conditions during the combustion of a paraffin mixture[3], then: $W_p \approx 28$ [g/mol], $W_{Air} \approx 29$ [g/mol], $T_1 \approx 2250$ [K], $T_{Air} \approx 288$ [K]. Substituting these values into the expression for β gives $\beta = 2.8445$. In the JFSH models, β is assumed to be equal to 2.85. (Note setting $\beta \approx 2.85$ is only valid for paraffins burning under typical atmospheric conditions as given above)[1]

By substituting the expression for $\xi(L_{B0})$ defined above in equation (15) and rearranging gives:

$$\boldsymbol{0.2 + 0.024 N_{\mathrm{Richardson}} L_{B0} + P_{2/3} L_{B0}^{-\frac{2}{3}} = 0} \qquad \textbf{(17)}$$

Where:

$N_{Richardson}$	=	$\left(\frac{g}{D_s^2 v_j^2}\right)^{\frac{1}{3}}$
$P_{2/3}$	=	$-\left(\frac{D_s \beta}{W_{st}}\right)^{\frac{2}{3}}$

Equation (17) is solved iteratively for L_{B0} using the Newton-Raphson procedure.

2.4 Calculation of angle between hole and flame axes (α)

Chamberlain[3] observed the angle between the hole and flame axes (α) (see Figure 1) to depend on the ratio (R) between the wind speed (Uw) and post-expansion jet velocity (vj) (i.e., R = Uw/vj). For $R \leqslant 0.05$, α is jet dominated, while in the range $R > 0.05$, α becomes increasingly dominated by wind forces. Chamberlain[3] gives two correlations which describe the behavior of α within these ranges of R. These are:

$$\boldsymbol{\alpha = \begin{cases} \dfrac{(8000R)}{N_{\mathrm{Richardson}} L_{B0}} + (\theta_{jv} - 90)\left(1 - e^{-25.6R}\right) & R \leq 0.05 \\ \dfrac{\left(1726\sqrt{R - 0.026} + 134\right)}{N_{\mathrm{Richardson}} L_{B0}} + (\theta_{jv} - 90)\left(1 - e^{-25.6R}\right) & 0.05 < R \end{cases}} \qquad \textbf{(18)}$$

In the absence of crosswind effects, θ_{jv} in equation (18) is replaced by θ_j (see Figure 1)[8]:

For the Johnson et al. model α can be easily obtained from plane geometry as (see Figure 3):

$$\boldsymbol{\alpha = cos^{-1}((X - B)/R_L)} \qquad \textbf{(19)}$$

Where R_L represents the frustum length (described later, see section 2.6).

[1] IMPROVE. Develop a generic method for calculating β for non-paraffins. This may involve the development of a database which stores values of T_1 and W_p for all major non-paraffinic combustible materials.

2.5 Frustum lift off

The 'frustum lift off', *B*, is defined as the distance along the hole axis from the hole to the point of intersection of the cone axis[3] (see Figure 1). Chamberlain[3] derived an expression that correlates *B* as a function of α and *R* in the range $0^o < \alpha < 180^o$. The expression is given by:

$$B = L_B \frac{sin\left(\left(0.185e^{-20R} + 0.015\right)\alpha\right)}{sin(\alpha)} \quad (20)$$

For $\alpha = 0^o$ or 180^o, *B* becomes:

$$B = \begin{cases} 0.2L_B & \alpha = 0^o \quad (still\ air) \\ 0.015L_B & \alpha = 180^o \quad (Lazy\ flames) \end{cases} \quad (21)$$

Note: the condition $\alpha = 180^o$ (i.e., "lazy" flames pointing directly into high winds[3]) can only occur for a horizontal release (see Figure 1)

For jet flames resulting from horizontal releases, Johnson et al. observed *B* to be directly proportional to the square root of the product of the local jet momentum and the local air density. Thus, *B* was found to be given by[4]:

$$B = 0.141\left(G_j \rho_{amb}\right)^{1/2} \quad (22)$$

Where:

$G_j = \pi \rho_j (r_j u_j)^2$

2.6 Calculation of the frustum length (R_L)

From Figure 1, the frustum length R_L, for the JFSH-Chamberlain and Cook models can be calculated from the geometrical relationship between R_L, L_B, α and *B* as:

$$R_L = \sqrt{L_B^2 - B^2 sin^2 \alpha} - B cos\, \alpha \quad (23)$$

Similarly, from Figure 3, R_L, for the JFSH-Johnson model can be determined from plane geometry as:

$$R_L = \sqrt{((X - B)^2 + Y^2 + Z^2)} \quad (24)$$

2.7 Calculation of width of frustum base (W_1)

Chamberlain found the width of the frustum base to correlate with *R* as[3]:

$$W_1 = D_s\left(13.5e^{-6R} + 1.5\right)\left(1 - \left(1 - \frac{1}{15}\sqrt{\frac{\rho_{amb}}{\rho_j}}\right)e^{-70R\xi(D_s)C}\right) \quad (25)$$

Where:

$\xi(D_S) = \left(\frac{g}{D_s^2 v_j^2}\right)^{\frac{1}{3}} D_s$

$C = 1000e^{-100R} + 0.8$

However, in the JFSH-Cook model the Cook et al. (1990) correlation for calculating the width of the frustum base is employed. It is given by[8]:

$$W_1 = D_s\left(13.5e^{-6R} + 1.5\right)\left(1 - \left(1 - \frac{1}{15}\sqrt{\frac{\rho_{amb}}{\rho_j}}\right)e^{-7.5R}\right) \quad (26)$$

Equation (26) is a simplification of equation (25). It was adopted in the Cook et al. (1990) model in order to overcome some form of numerical instability when calculating W_1 at very low wind speeds[11].

For jet flames resulting from horizontal vapour phase releases, Johnson et al. found W_1 to correlate with the B and $\xi(L_{B0})$ as[4]:

$$W_1/B = -0.18 + 0.081\xi(L_{B0}) \quad (27)$$

Equation (27) is subject to the following constraint: $W_1/B \geqslant 0.12$

2.8 Calculation of width of frustum tip (W_2)

For the JFSH-Chamberlain and Cook models, the correlation developed by Chamberlain, which expresses the width of the frustum tip (W_2) as a function of R and L_B is employed. It is given by[3]:

$$W_2 = L_B\left(0.18e^{-1.5R} + 0.31\right)\left(1 - 0.47e^{-25R}\right) \quad (28)$$

For jet flames resulting from horizontal vapour phase releases, Johnson et al. found W_2 to correlate with Ω_x and $\xi(L_{B0})$ as[4]:

$$W_2/Lb_{xy} = -0.004 + 0.0396\xi(L_{B0}) - \Omega_x\left(0.0094 + 9.5\times10^{-7}\left(\xi(L_{B0})\right)^5\right) \quad (29)$$

Where:

$$Lb_{xy} = \left(X^2 + Z^2\right)^{1/2} \quad (30)$$

Equation (29) is subject to the following constraint: $Lb_{xy} \geqslant W_2 \geqslant W_1$

The above equations define the flame dimensions and orientation in space. The estimation of the flame's surface emissive power is described below.

2.9 Surface emissive power ($W_{surface}$)

The surface emissive power (SEP) [W/m^2] is the heat flux due to heat radiation across a flame's surface area. For a jet flame, the surface emissive power can be expressed as[3]:

$$W_{\text{Surface}} = \frac{F_s m H_{COMB}}{A} \quad (31)$$

Where:

F_s	=	Fraction of heat radiated from the surface of the flame [-]
m	=	Mass discharge rate [kg/s]
H_{COMB}	=	Heat of combustion of the fuel mixture [J/kg]
A	=	Total surface area of the flame (conical frustum) [m^2]

The predicted surface emissive power is limited to a maximum value which could be set based on experimental data or engineering judgement. The previous current default value (Phast 7.2 and Safeti 6.7) for the maximum surface emissive power was 400kW/m^2, and has been reduced to 350 kW/m^2 in subsequent releases following correspondence with Chamberlain (2011)[12].

Chamberlain found F_s to correlate with gas post-expansion velocity (v_j) as:

$$F_s = 0.21e^{-0.00323v_j} + 0.11 \quad (32)$$

However, the JFSH-Cook model makes use of a modified expression for F_s, which expresses the latter as a function of the fluid's post-expansion velocity (v_j) and molecular weight (M_W). It is given by:

$$F_S = \begin{cases} 0.21e^{-0.00323v_j} + 0.11 & M_W < 21 \\ \left(0.21e^{-0.00323v_j} + 0.11\right)\sqrt{\frac{M_W}{21}} & 21 \le M_W \le 60 \\ 1.69\times\left(0.21e^{-0.00323v_j} + 0.11\right) & 60 < M_W \end{cases} \quad (33)$$

Experimental evidence suggests that F_S increases with M_W[14,13] Equation (33) is an improvement on equation (32) as it better approximates (based on available jet flame data) the effect of heavier releases (M_W > 21) on the predicted value of F_S.

Johnson et al. found flame SEP to vary with average emitting path-lengths through the flame. The authors suggest different values of F_S and SEP for the ends and sides of the flame. The overall behaviour of the flame as a radiant energy source was found to be better correlated as a function of W_2 and/or R_L depending on the location of the observer. W_2 and R_L where chosen as representative path-lengths for emission through the sides and ends of the model flame shape respectively. Thus, expressions for F_S and SEP for the sides and ends of a jet flame are given by[4]:

Emission through flame sides:

$$F_s^{SIDE} = \left(1 - e^{-0.4W_2}\right)\left(0.21e^{-0.00323v_j} + 0.14\right) \quad (34)$$

$$W_{Surface}^{SIDE} = \frac{F_s^{SIDE} m H_{COMB}}{A} \quad (35)$$

Emission through flame ends:

$$F_s^{END} = \left(1 - e^{-0.4R_L}\right)\left(0.21e^{-0.00323v_j} + 0.14\right) \quad (36)$$

$$W_{Surface}^{END} = \frac{F_s^{END} m H_{COMB}}{A} \quad (37)$$

$W_{Surface}^{SIDE}$ and $W_{Surface}^{END}$ represent the flame's SEP as experienced by observers whose view is respectively restricted to the sides and ends of the flame. $W_{Surface}^{SIDE}$ is adopted as a representative value for the overall flame SEP in the JFSH-Johnson model.

From geometry, the total surface area of the conical frustum (i.e., including its end discs) can be expressed as:

$$A = \frac{\pi}{4}\left(W_1^2 + W_2^2\right) + \frac{\pi}{2}(W_1 + W_2)\sqrt{R_L^2 + \frac{1}{4}(W_2 - W_1)^2} \quad (38)$$

2.10 The flame co-ordinates

The flame simulated by the JFSH models is always defined by four circles. Each circle is defined by four co-ordinates, the x and z co-ordinate of the centre of the circle, the radius of the circle and the inclination of the circle. The first and second circles and the third and fourth circles have the same centre and inclination respectively. The first and fourth circles have zero radii.

The x-axis of the above [x, y, z] Cartesian co-ordinate system corresponds to the horizontal projection of the flame axis along the vertical plane cutting the jet flame into symmetrical halves (i.e. the [x-z] plane). The x co-ordinate of each circle is taken with respect to a virtual origin located along the [x-z] plane. The virtual origin corresponds to the orthogonal projection of the release source on the [x-z] plane[2].The z co-ordinate of the centre of each circle corresponds to its vertical height above the x-axis.

The calculation of the x co-ordinate of each circle requires the knowledge of the angle (ϕ_{flame}) between the vertical plane cutting the release source into symmetrical halves (i.e. the [X-Z] plane) [3] and the [x-z] plane. These planes intersect along a vertical line passing through the centre of the flame's frustum base. From geometry, the (X, Y) co-ordinate set of the centre of the frustum tip with respect to the centre of the frustum base (i.e. the adopted origin of the [X, Y, Z] Cartesian co-ordinate system) can be derived as:

For the JFSH-Cook and Chamberlain models:

[2] This axis transformation permits the easy and accurate incorporation of crosswind effects in jet fire radiation calculations (i.e. JFSH-EXPS model)

[3] Here we define a new [X, Y, Z] Cartesian co-ordinate system whose co-ordinates are expressed in terms of upper case characters (see Figure 3)The X axis corresponds to the projection of the release axis on the horizontal plane. Thus, the vertical or [X-Z] plane corresponds to the plane in which Y = 0. For a vertical release, the X axis is defined as the geographical East direction.

$$(X_2, Y_2) = \left(\frac{R_L}{\sin\theta_{jv}}\left[\sin(\theta_{jv} - \alpha)\cos\theta_j + \sin\alpha\cos f\right], \frac{R_L}{\sin\theta_{jv}}\sin\alpha\sin f\right) \rightleftarrows \theta_j \neq 0$$

$$(X_2, Y_2) = \begin{cases} (R_L\cos\alpha, R_L\sin\alpha) & \theta_j = 0; f \geq 0 \\ (R_L\cos(-\alpha), R_L\sin(-\alpha)) & \theta_j = 0; f < 0 \end{cases} \quad (39)$$

For the JFSH-Johnson model

$$(X_2, Y_2) = ((X - B), Y) \quad (40)$$

Thus, the angle ϕ_{flame} can be calculated as:

$$\varphi_{flame} = \tan^{-1}(Y_2/X_2) \quad (41)$$

Hence, the co-ordinate sets for each circle for the JFSH-Cook, Chamberlain and Johnson models along the vertical plane cutting the flame into symmetrical halves can be defined using the following intermediate variables (see Figure 1) as:

$$(x_1, z_1) = \left(B\left|\cos\theta_j\cos\varphi_{flame}\right|, B\sin\theta_j\right) - 90 \leq \theta_j \leq 90 \quad (42)$$

$$(x_2, z_2) = (x_1 + R_L\cos\lambda, z_1 + R_L\sin\lambda) - 90 \leq \theta_j \leq 90; 0 \leq \theta_{jv} \leq 180 \quad (43)$$

Where:

For the JFSH-Cook and Chamberlain models:

$$\lambda = \sin^{-1}\left(\frac{\sin\theta_j\left(\sin(\theta_{jv} - \alpha)\right)}{\sin\theta_{jv}}\right) \quad (44)$$

For the JFSH-Johnson model λ is given by:

$$\lambda = \sin^{-1}(Z_2/R_L) \quad (45)$$

From geometry, the inclination of the circles (ϑ) relative to the horizontal plane is derived as:

$$\vartheta = |90 - \lambda| - 90 \leq \theta_j \leq 90; 0 \leq \theta_{jv} \leq 180 \quad (46)$$

Thus, the vector (co-ordinates) representing each circle is given by:

$$r_1 = (x_1, z_1 + z_{Elev}, 0, \vartheta) \quad (47)$$

$$r_2 = \left(x_{1,}, z_1 + z_{Elev}, \frac{1}{2}W_1, \vartheta\right) \quad (48)$$

$$r_3 = \left(x_2, z_2 + z_{Elev}, \frac{1}{2}W_2, \vartheta\right) \quad (49)$$

$$r_4 = (x_2, z_2 + z_{Elev}, 0, \vartheta) \quad (50)$$

Where:

z_{Elev}	=	Elevation of the release point (e.g., flare tip) from the horizontal plane [m]
x_1	=	Horizontal distance of the frustum base from the virtual origin along the vertical plane cutting the flame into symmetrical halves [m]
x_2	=	Horizontal distance of the frustum tip from the virtual origin along the vertical plane cutting the flame into symmetrical halves [m]
z_1	=	Vertical distance of the frustum base from the virtual origin along the vertical plane cutting the flame into symmetrical halves [m]
z_2	=	Vertical distance of the frustum tip from the virtual origin along the vertical plane cutting the flame into symmetrical halves [m]
ϑ	=	Inclination of the frustum base relative to the horizontal plane [°]
ϕ	=	Angle between the wind vector and the projection of the release axis on the horizontal plane [°]
ϕ_{flame}	=	Angle between the vertical planes cutting the release source and jet flame respectively into symmetrical halves [°]

2.11 Determination of likelihood of flame touch down or on-ground impingement

Flame touch down is said to occur if any of the sides of the conical frustum possesses an elevation less or equal to zero. The lowest point on the conical frustum lies at the edges of the frustum in the vertical plane that cuts the frustum into symmetrical halves. From geometry, the elevation and horizontal distances (relative to the virtual origin) of the lower ends of the frustum base (x_{base}, z_{base}) and tip (x_{tip}, z_{tip}) (see Figure 8), along the vertical plane cutting the frustum into symmetrical halves can be expressed as:

$$x_{tip} = x_1 + R_L \cos\lambda + \left(\frac{W_2}{2}\right)\sin\lambda \quad (51)$$

$$x_{base} = x_1 + \left(\frac{W_1}{2}\right)\sin\lambda \quad (52)$$

$$z_{tip} = z_2 - \left(\frac{W_2}{2}\right)\cos\lambda \quad (53)$$

$$z_{base} = z_1 - \left(\frac{W_1}{2}\right)\cos\lambda \quad (54)$$

In the event that z_{base} or z_{tip} is less than zero, the exact point of on-ground impingement (x_{impg}, 0) relative to the virtual origin can be determined from linear interpolation as:

For $z_{base} \leqslant 0$

$$x_{impg} = x_{base} + \frac{x_{base} z_{base}}{(z_1 - z_{base})} \quad (55)$$

For $z_{tip} \leqslant 0$

$$x_{impg} = x_{tip} - \frac{(x_{base} - x_{tip}) z_{tip}}{(z_{base} - z_{tip})} \quad (56)$$

The distance of the point of on-ground impingement (X_{impg}) from the release point can be expressed as:

$$X_{impg} = \sqrt{\left[B\cos\theta_j + (x_{impg} - x_1)\cos\varphi_{flame}\right]^2 + \left[(x_{impg} - x_1)\sin\varphi_{flame}\right]^2} \quad (57)$$

3 THE LIQUID/TWO-PHASE JET FIRE MODEL

3.1 Effective Source Diameter

The jet flame resulting from a liquid/two-phase release is modelled using a modified form of the JFSH-Cook pure vapour jet fire model. Apart from the expression employed in calculating the flame's effective source diameter (D_s), the correlations defining flame dimensions, fraction of heat radiated and surface emissive power for the vapour and liquid/two-phase jet fire models are essentially the same.

Based on experimental evidence on the behaviour of jet flames following condensate releases[14], liquid/two-phase jet fires are modelled by determining a gas flame having the same release rate and initial momentum as the liquid/two-phase release. The flame's effective source diameter is given by:

$$D_s = 2r_j\sqrt{\frac{\rho_j}{\rho_{vap}[T_{sat}(P_o)]}} \quad (58)$$

Here $\rho_{vap}[T_{sat}(P_o)]$ equals the saturated vapour density of the fuel at ambient pressure [kg/m^3]. Furthermore, D_s represents the diameter of a hole that gives the same exit velocity for the release of the material as a gas. D_s, $\rho_{vap}[T_{sat}(P_o)]$ (used in place of ρ_j), v_j and prevailing ambient conditions are employed in the JFSH-Cook vapour phase model in determining the flame shape.

For some materials, particularly mixtures, liquid density could be returned as vapour density by property calculation if the saturation temperature at atmospheric pressure is very low and this would subsequently lead to under-predictions of jet fire radiation. This is prevented now by using ideal gas density if no valid vapour density is found by the property calculation for a 2-phase discharge.[4]

3.2 Mass discharge rate – two phase releases

For two-phase releases, not all liquid mass may contribute to the 2-phase jet fire. Although representing different physics, it is envisaged that an indication of this for linked jet fire calculations is given by the rainout mass fraction $\eta_{rainout}$ predicted by the UDM model. Following consultation with the users and in analogy with the fireball and explosion model assumptions, the flammable mass is taken to be as given by equation (59) with the default value for the jet fire parameter $r_{jetmass}$=3. This will lead to $m=M_d$ for rainout fractions less than 2/3. Also m gradually reduces to 0 if the amount of rainout approaches 100%.

$$\mathbf{m} = \boldsymbol{M_d}\, \boldsymbol{min}\left[\mathbf{1}, \boldsymbol{r_{jetmass}}(\mathbf{1} - \boldsymbol{\eta_{rainout}})\right] \tag{59}$$

Time-varying discharge

For time-varying releases the discharge rate M_d varies with time. In analogy with the above equation the mass contributing to the two-phase jet fire for each time i is estimated as

$$\boldsymbol{M^i} = \boldsymbol{M_d}^{\boldsymbol{i}}\, \boldsymbol{min}\left[\mathbf{1}, \boldsymbol{r_{jetmass}}(\mathbf{1} - \boldsymbol{\eta_{rainout}}^{\boldsymbol{i}})\right] \tag{60}$$

Where

M_d^j = mass release rates for record i [kg/s]
$\eta_{rainout}^j$ = rainout mass fraction for record i (kg/kg)

The mass discharge rate m used for the jet fire calculations is the average of M^i over the jet fire average time t_{jet} (default value 20 seconds):

$$\boldsymbol{m} = \frac{\sum_{i=1}^{j} \boldsymbol{M^i}\ \ \boldsymbol{t_i} + \boldsymbol{M^{j+1}}\ \ (\boldsymbol{t_{jet}} - \sum_{i=1}^{j} \boldsymbol{t_i})}{\boldsymbol{t_{Jet}}} \tag{61}$$

Here t_i equals the duration (s) of segment i. Furthermore t_{jet} is the jet fire average time (default value 20 seconds). Furthermore segment j+1 is the discharge segment at which the jet fire averaging time j is achieved, i.e.

$$\sum_{i=1}^{j} t_i < t_{jet} < \sum_{i=1}^{j+1} t_i$$

The above applies for jet overall release duration t_{tot} larger than t_{jet}. For duration t_{tot} less than j_{jet}, the jet averaging time of t_{tot} is applied.

4 THE MILLER (M-MPS) JET FIRE MODEL FOR LOW-LUMINOSITY GASES

4.1 Introduction

The Miller model is an extension of JFSH-Chamberlain/Johnson models to low-luminosity/non-hydrocarbon jet flames from flare stacks inclined horizontally, vertically or 45° to the horizontal.

Instead of a cone, the flame is represented as a line source with two distinct straight line segments. The first segment near the release is projected in the direction of the release itself. The second segment is angled according to uplift due to buoyancy, tilt due to the wind and/or sideways due to a crosswind.

[4] IMPROVE. For multi-component mixtures one should ideally use the vapour density at the bubble point, $\rho_{vap}[T_{bubble}(P_o)]$ instead of the saturated vapour density, $\rho_{vap}[T_{sat}(P_o)]$ since the latter is ill-defined for MC mixtures.

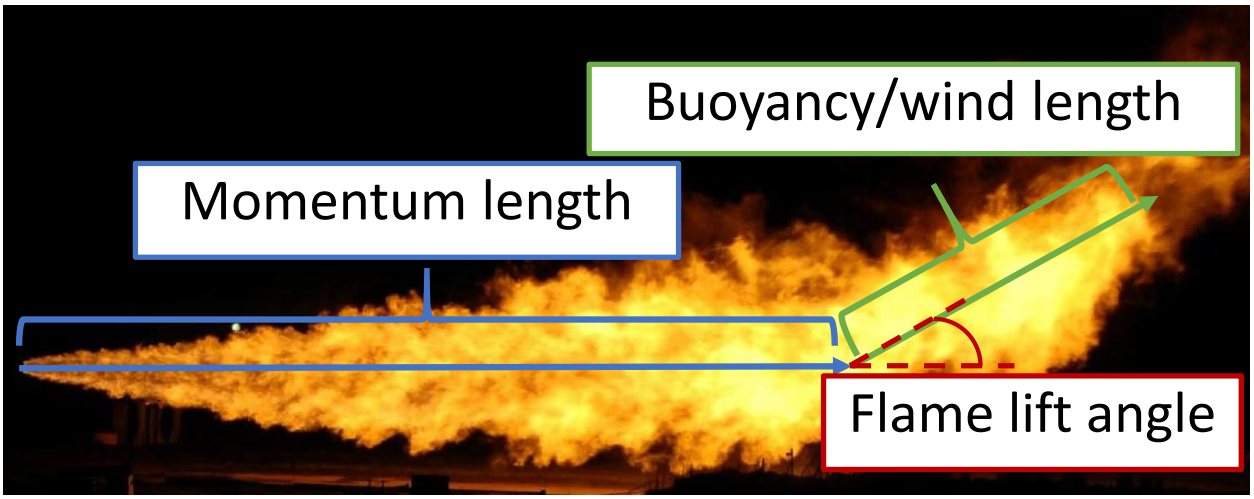

Figure 4 **Miller model flame representation for horizontal jet fires**

The different release orientations are illustrated in Figure 4 and Figure 5.

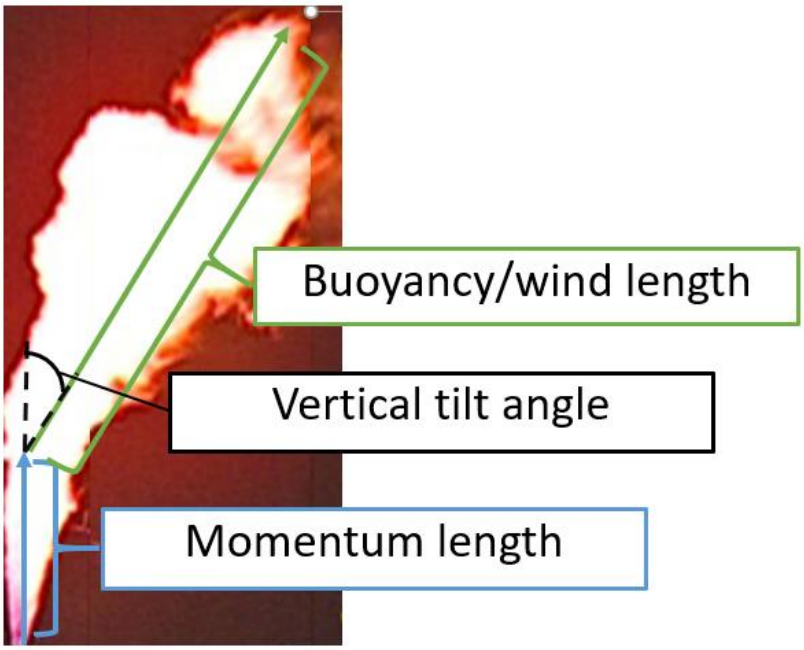

Figure 5 **Miller model flame representation for vertical jet fires**

With respect to radiation this is considered to be emitted along the flame centreline with an intensity distribution that rises and falls in a linear fashion with a maximum at a distance corresponding to 2/3 of the overall flame length. This concept is illustrated in Figure 6.

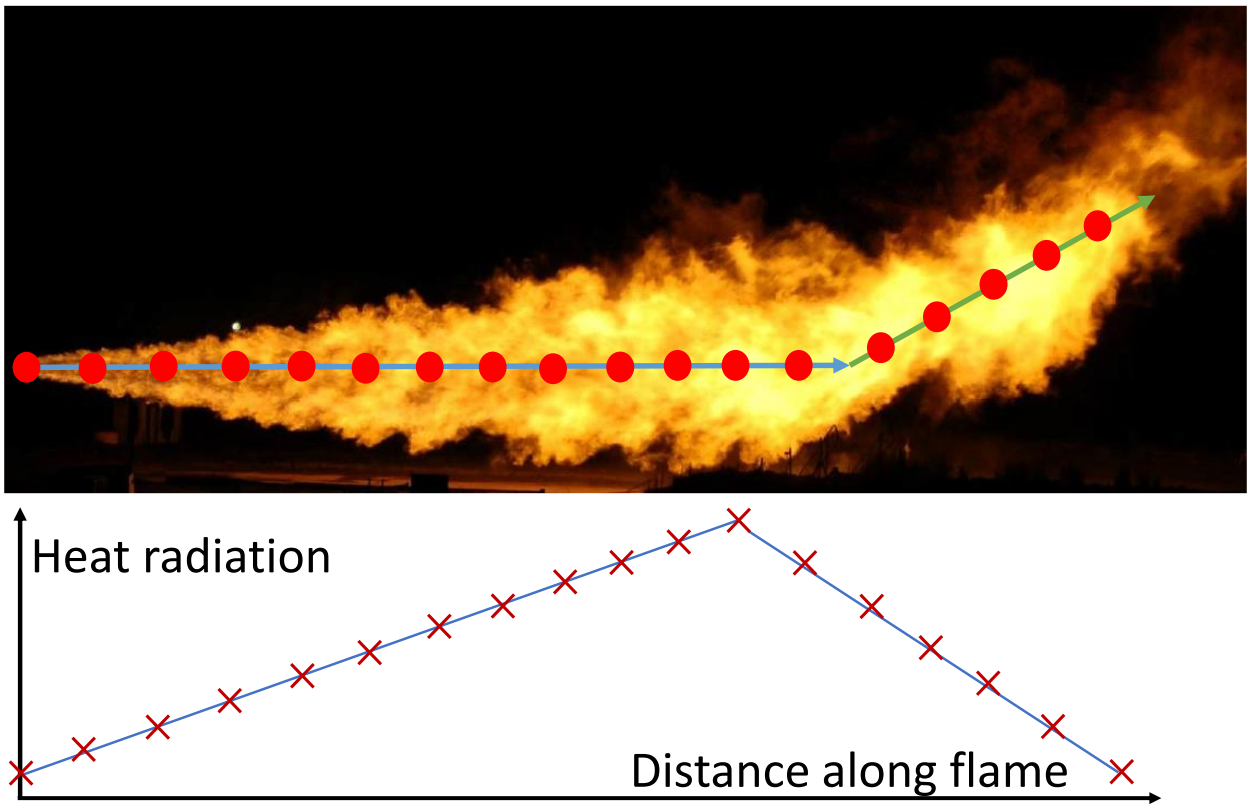

Figure 6 **Miller model radiation intensity distribution**

In this document we refer to this model formulation as M(iller)-(M)ulti (P)oint (S)ource model, M-MPS.

In spite of the apparent differences in formulation between the Miller and Cone models, this model is using the Chamberlain model as it's basis. The key modifications applied in M-MPS to JFSH-Chamberlain/Johnson models can be summarized under the following broad topics:

- Calculation of wind velocity at flare tip
- Calculation of still air flame length parameters for non-hydrocarbon/low-luminosity gases
- Calculation of angle between flame axis (flame tilt or lift) and the horizontal
- Calculation of flame momentum and lift-off distances
- Calculation of flame centreline, hole-to-tip and frustum lengths
- Calculation of flame radiant heat fraction and radiation characteristics
- Flame (centreline) co-ordinates

In addition, the M-MPS model implemented in Phast/Safeti has been extended to support the following:

- Determination of equivalent natural gas flowrate for vertical flame tilt angle calculation
- Modelling of crosswind impact for non-vertical releases
- Modelling of radiation impact on planar observers
- Application of numerical integrators for radiation effect modelling
- Finite flame lift off distance and height relative to release location

- Application of the HyRAM radiative fraction correlation

Note that in the implementation of the M-MPS model, any releases with:

- $\theta_j > \pi/3$ is modelled using the vertical inclination logic,
- $\theta_j < 0.16\pi$ is modelled using the horizontal inclination logic,
- $0.16\pi < \theta_j < \pi/3$ is modelled using the 45° inclination logic

4.2 Calculation of wind speed at flare tip (U_w)

The M-MPS model assumes wind speed at the flare tip (U_w) to vary with flare stack height above a reference height (h_0) of 10m. The relationship between wind speed at reference height ($U_{w,0}$) and actual wind speed at flare tip follows a power-law profile given by:

$$\boldsymbol{U_w = U_{w,0}\left(\frac{z_{Elev}}{h_0}\right)^{aw}} \quad \textbf{(62)}$$

Where:

h_0	=	Reference height for the measurement of wind velocity, assumed as 10m [m]
$U_{w,0}$	=	Wind speed measured at reference height [m/s]
aw	=	Power law exponent, dependent on ground roughness of surrounding terrain

4.3 Calculation of still air flame length parameters for non-hydrocarbons

The M-MPS model employs the Kalghatgi correlation (see equation (15)) in determining the still air flame length (L_{B0}) for non-hydrocarbon flames. For flammable materials, the key parameters in Kalghatgi's correlation may be determined as:

- Mass fraction of fuel in stoichiometric mixture with air (W_{st}):

$$\boldsymbol{W_{st} = \frac{M_W C_t}{C_t\ M_W + (1 - C_t)W_{Air}}} \quad \textbf{(63)}$$

- Mean product molecular weight (W_p) [kg/kmol]:

$$\boldsymbol{W_p = A_t(C_t\ M_W + (1 - C_t)W_{Air})} \quad \textbf{(64)}$$

Where:

$$C_t = \frac{moles\ of\ \ fuel}{moles\ of\ \ fuel + moles\ of\ air} \quad \textbf{(65)}$$

$$A_t = \frac{moles\ of\ \ fuel + moles\ of\ air}{moles\ of\ combustion\ products} \quad \textbf{(66)}$$

- Adiabatic combustion temperature (T_1) [K]: Miller (2017) presented the following correlations for estimating adiabatic combustion temperature for mixtures containing flammable and inert gases,

$$\boldsymbol{T_1 = T_{1,fuel}\left(-0.7395CD_{equiv}^2 + 0.0366CD_{equiv} + 0.9972\right)} \quad \textbf{(67)}$$

$$\boldsymbol{T_{1,fuel} = 321.08H_{2equiv}^3 - 310.88H_{2equiv}^2 + 144.03H_{2equiv} + 2223} \quad \textbf{(68)}$$

$$CD_{equiv} = x_{CD} + 0.84x_{WA} + 0.59x_{N2} \quad (69)$$

$$H_{2equiv} = \frac{x_{H2equiv}}{x_{H2equiv} + x_{C1equiv}} \quad (70)$$

$$x_{H2equiv} = x_{H2} + x_{CM} \quad (71)$$

$$x_{C1equiv} = x_{C1} + x_{C2} + x_{C3} + x_{C4} + x_{C..} \quad (72)$$

Where:

$T_{1,fuel}$	=	Adiabatic combustion temperature for combustible materials [K]
X_{CD}, X_{WA}, X_{N2}	=	Mole fractions of Carbon dioxide, water vapour and Nitrogen in fuel mixture [-]
$X_{H2equiv}$	=	Sum of mole fractions of flammable non-hydrocarbons [-]
$X_{C1equiv}$	=	Sum of mole fractions of flammable hydrocarbons [-]
X_{H2}, X_{CM}	=	Mole fractions of Hydrogen and Carbon monoxide [-]
$X_{C1,C2,C3,C4,C..}$	=	Mole fractions of hydrocarbons [-]

4.4 Angle between flame axis (flame tilt or lift) and the horizontal, α_{AP}

For vertical releases, Miller (2017) proposed the following momentum correction to the Chamberlain flame tilt correlation originally developed for natural gas flames (see equation (18)):

$$a_{AP,vert} = MAX\left(0, MIN\left(a\frac{\dot{m}_{NG}}{m}, \frac{\pi}{2}\right)\right) \quad (73)$$

Where:

$\alpha_{AP,vert}$	=	Angle between flame axis and the hole axis [°]
$\dot{m}_{NG}$	=	Mass flowrate of natural gas that gives the same L_{B0} as the gas of interest, for the same flare diameter (d_0) [kg/s]

Miller (2017) gives the following correlations for estimating $\dot{m}_{NG}$ in terms of the flare diameter (d_0)[5]:

$$\dot{m}_{NG} = 255.42 d_0^2 Y_{NG} \quad (74)$$

$$Y_{NG} = \begin{cases} 2.0074X_{NG}^2 - 1.0103X_{NG} + 0.0185, & X_{NG} > 0.665 \\ 0.7873X_{NG}^{2.9013}, & X_{NG} \leq 0.665 \end{cases} \quad (75)$$

$$X_{NG} = \frac{L_{B0}}{174.83 d_0^{0.8794}} \quad (76)$$

As such, the angle between the flame axis and the horizontal (α_{AP}) for vertical releases is given by:

$$a_{AP} = \frac{\pi}{2} - a_{AP,vert} \quad (77)$$

For releases inclined at 45° from the horizontal, $\alpha_{AP} = \pi/4$, i.e., the ensuing jet flame is assumed to be straight, continuing at ca 45° from flare tip to flame end tip (Miller, 2017).

For horizontal releases, Miller (2017) gives the following correlation for the horizontal lift angle (i.e., α_{AP}):

$$a_{AP} = MAX\left(0, MIN\left\{\sin^{-1}\left(\frac{z_2}{L_f - B_M}\right), \left(\frac{\pi}{2} - a_{AP,vert}\right)\right\}\right) \quad (78)$$

[5] NOTE: From a review of Kalghatgi's correlation for L_{B0} (equation (15)), it is possible to show that there are a family of natural gas flowrates that give the same L_{B0} for a fixed d_0. It is also possible to show that $1/D_{s,NG}^{2/3}$ varies linearly with $-1/\dot{m}_{NG}^{2/3}$ for a fixed d_0.

Where:

L_f	=	Flame centreline length [m]
$\alpha_{AP,vert}$	=	Flame tilt from vertical for the same flame released vertically [°]
z_2	=	Horizontal flame lift due to buoyancy (see Figure 1 and Figure 3) [m]
B_M	=	momentum dominated flame length measured from release point [m]

Where L_f, z_2 and B_M, respectively, are given by[6]:

$$\boldsymbol{L_f = B_M + R_L} \quad \textbf{(79)}$$

$$\boldsymbol{z_2 = MAX\left(0, MIN\left(0.05 N_{Richardson} L_{B0}, 1\right)\right)} \quad \textbf{(80)}$$

$$\boldsymbol{\frac{B_M}{L_{B0}} = MAX\left(0, MIN\left(e^{-0.13 N_{Richardson} L_{B0}}, 1\right)\right)} \quad \textbf{(81)}$$

Equation (78) implies that the maximum lift angle for horizontal releases is capped at the flame tilt relative to the horizontal ($\pi/2 - \alpha_{AP,vert}$) for the same flame if released vertically[7].

4.5 Calculation of flame momentum (B_M) and lift-off (B) distances

For releases inclined vertically or at 45° to the horizontal, the momentum dominated flame length (B_M) is calculated from equations (20) and (21), but with $\alpha_{AP,vert}$ employed in place of α (Miller, 2017) [8].

For horizontal releases, flame lift off distance is calculated from equation (81).

Miller (2017) assumes jet flames to burn very close to source, i.e., with zero flame lift off distance (B).

4.6 Flame centreline (L_f), hole-to-tip (L_B) and frustum (R_L) lengths

The flame centreline length (L_f) is given by equation (79). For releases inclined horizontally or at 45° to the horizontal, Miller (2017) recommends setting L_f equal to L_{B0}, i.e.,

$$\boldsymbol{L_f = L_{B0} = B_M + R_L} \quad \textbf{(82)}$$

For vertical releases, the frustum length (R_L) is calculated from equation (23), but with $\alpha_{AP,vert}$ employed in place of α (Miller, 2017). For releases inclined horizontally or at 45° to the horizontal, R_L is simply determined from equation (82), i.e.:

$$\boldsymbol{R_L = L_{B0} - B_M} \quad \textbf{(83)}$$

From geometry and assuming the buoyant portion of the flame is blown crosswind in the direction (φ_{flame}) relative to the release plane (see section 4.9), the flame hole-to-tip length (L_B) may be calculated for releases inclined horizontally, or at 45° to the horizontal, as:

$$\boldsymbol{L_B = \begin{cases} \sqrt{z_2^2 + B_M^2 + (R_L \cos \alpha_{AP})^2 + 2 R_L B_M \cos \alpha_{AP} \cos \varphi_{flame}}, & \textit{Horizontal} \\ \sqrt{z_2^2 + (\cos \alpha_{AP})^2 \left(B_M^2 + R_L^2 + 2 R_L B_M \cos \varphi_{flame}\right)}, & 45° \textit{ inclined} \end{cases}} \quad \textbf{(84)}$$

[6] NOTE: Equations (80) and (81) differ from equations published in Miller (2017). These correspond to correlations employed in the current implementation of AP Flame (provided via private communication with Miller, D., February 2021). The equations for z_2 and B_M as published in Miller (2017) are given by: $\frac{z_2}{L_{B0}} = 0.125 N_{\text{Richardson}} L_{B0} - 0.25, 0 \leq \frac{z_2}{L_{B0}} \leq 1$ and $\frac{B_M}{L_{B0}} = -0.125 N_{\text{Richardson}} L_{B0} + 1.25, 0 \leq \frac{B_M}{L_{B0}} \leq 1$. Equations (80) and (81), as implemented in AP Flame, supersede published correlations in Miller (2017).

[7] CLARIFY: It is not clear why the constraint on maximum horizontal tilt is not applicable to releases inclined at 45° to the horizontal, i.e., equation (78) with $\alpha_{AP} = MAX\left(0, MIN\left\{\frac{\pi}{4}, \left(\frac{\pi}{2} - \alpha_{AP,vert}\right)\right\}\right)$. On the other hand, if $\alpha_{AP} = \pi/4$ for all releases inclined at 45° to the horizontal, irrespective of wind speed, it would seem logical that the maximum lift angle for horizontal releases, should not exceed $\pi/4$.

[8] CLARIFY: For releases inclined at 45° to the horizontal, the flame lift-off distance is calculated using $\alpha_{AP,vert}$ derived from equation (73) before α_{AP} is set to $\pi/4$. It is not clear why the seeming inconsistency.

For vertical releases, Miller (2017) recommends applying the Chamberlain correlation in calculating L_B, i.e., equation (4), for scenarios with $\alpha_{AP,vert} < \pi/3$. Otherwise, L_B should be determined using the following correlations:

$$\frac{L_B}{L_{B0}} = ae^{ba_{AP,vert}}, \quad \frac{p}{3} \leq a_{AP,vert} \leq \frac{p}{2} \tag{85}$$

Where:

$$a = e^{-90b} \tag{86}$$

$$b = \frac{1}{30}\ln\left(\frac{1}{(L_B/L_{B0})_{60}}\right) \tag{87}$$

$$(L_B/L_{B0})_{60} = 0.49 + 0.51e^{-0.4U_{W,60}} \tag{88}$$

$$U_{W,60} = R_{60}v_j \tag{89}$$

$$R_{60} = \begin{cases} 0.026 + \left(\left(60N_{Richardson}L_{B0}\frac{m}{\dot{m}_{NG}} - 134\right)/1726\right)^2, & for \ \frac{60N_{Richardson}L_{B0}m}{\dot{m}_{NG}8000} > 0.05 \\ \frac{60N_{Richardson}L_{B0}m}{\dot{m}_{NG}8000}, & for \ \frac{60N_{Richardson}L_{B0}m}{\dot{m}_{NG}8000} \leq 0.05 \end{cases} \tag{90}$$

4.7 Calculation of radiant heat fraction and radiation characteristics

Miller (2017) recommends the following correlation for determining the total heat radiating from the flame along the flame centreline (Q_{rad}):

$$Q_{rad} = F_{AP}mH_{COMB} \tag{91}$$

Where:

F_{AP} = Flame radiant heat fraction along the flame centreline [-]

$$F_{AP} = MAX\{(x_{C1equiv}F_s + x_{H2equiv}F_{H2}), 0.05\} \tag{92}$$

F_s, $x_{H2equiv}$ and $x_{C1equiv}$ are given by equations (32), (71)and (72), respectively, while F_{H2} is given by:

$$F_{H2} = F_{corr}(0.1691 - 0.01\ln(M_{flux})) \tag{93}$$

Where:

$$M_{flux} = \frac{4m}{pd_0^2} \tag{94}$$

$$F_{corr} = \begin{cases} 1, & for\ vertical \\ 1.36 + 0.076MIN\{10, L_f/h_{RC}\}, & for\ horizontal/45° \end{cases} \tag{95}$$

$$h_{RC} = \begin{cases} z_{Elev} + MAX(0, (0.66L_f - B_M)\sin(a_{AP})), & for\ horizontal \\ z_{Elev} + 0.66L_f\sin\left(\frac{p}{4}\right), & for\ 45° \end{cases} \tag{96}$$

The radiated heat is assumed to be generated from point sources evenly distributed along the flame centreline (L_f). The amount of heat from each point source is linearly weighted with minimum values at each end and a maximum at the radiant centre of the flame, 2/3 along L_f (Miller, 2017).

4.8 Calculation of equivalent natural gas flowrate using similarity approach

As indicated in section 4.4, the correlations proposed by Miller (2017) for estimating $\dot{m}_{NG}$, i.e., equations (74) to (76) may not give a unique solution. In essence, it is possible to show that there are a family of natural gas flowrates that give the same L_{B0} for a fixed d_0.

As a result, an alternative approach for determining $\dot{m}_{NG}$, based on similarity considerations, has been developed. In this approach, $\dot{m}_{NG}$ corresponds to the mass flowrate of natural gas that gives the same L_{B0} and uncorrected (Chamberlain) flame tilt, α, as the gas of interest.

From equations (15) and (18), this implies that:

$$\frac{\boldsymbol{D_s\beta}}{\boldsymbol{W_{st}}} = \frac{\boldsymbol{D_{s,NG}\beta_{NG}}}{\boldsymbol{W_{st,NG}}} \quad \textbf{(97)}$$

$$\frac{\mathbf{1}}{\boldsymbol{D_s^2 v_j^2}} = \frac{\mathbf{1}}{\boldsymbol{D_{s,NG}^2 v_{j,NG}^2}} \quad \textbf{(98)}$$

From equations (97) and (98), the equivalent natural gas source diameter ($D_{s,NG}$) and post-expansion velocity $v_{j,NG}$ can be calculated as:

$$\boldsymbol{D_{s,NG}} = \frac{\boldsymbol{W_{st,NG} D_s \beta}}{\boldsymbol{W_{st}\beta_{NG}}} \quad \textbf{(99)}$$

$$\boldsymbol{v_{j,NG}} = \sqrt{\frac{\boldsymbol{D_{s,NG}^2}}{\boldsymbol{D_s^2 v_j^2}}} \quad \textbf{(100)}$$

As such, $\dot{m}_{NG}$, can be calculated from $D_{s,NG}$, $v_{j,NG}$ and ρ_{amb} as:

$$\boldsymbol{\dot{m}_{NG}} = \boldsymbol{\rho_{amb} v_{j,NG} \pi \frac{D_{s,NG}^2}{4}} \quad \textbf{(101)}$$

Note that $W_{st,NG}$ and β_{NG} are calculatable quantities for a fixed natural gas mixture, see equations (63) to (66)[9].

4.9 Modelling of crosswind impact for non-vertical releases

The M-MPS model intrinsically accounts for crosswind impact for vertical releases given that the buoyant portion of the flame (R_L) will orient in the direction of the prevailing wind (ϕ).

However, the Miller (2017) model does not account for crosswind impact on non-vertical releases. To address this limitation, the M-MPS model has been extended to support two methods for modelling crosswind impact, these are:

- The “full-deflection” approach: In this method, the buoyant portion of the flame, as with vertical releases, is assumed to orient in the direction of the prevailing wind (ϕ), i.e.:

$$\boldsymbol{\varphi_{flame}} = \boldsymbol{\phi} \quad \textbf{(102)}$$

- The “modified Johnson” approach[10]: In this method, the orientation of the buoyant portion of the flame is calculated from equation (41), based on the Johnson methodology, where:

[9] NOTE: by default, the properties of natural gas is based on pure (100%) Methane.
[10] NOTE: default and only option available in Phast/Safeti

$$Y_2 = Y = X_2 0.178\Omega_y \quad (103)$$

$$X_2 = \begin{cases} \sqrt{\dfrac{MAX\left(\left(L_f - B_M\right)^2 - z_2^2, 0\right)}{1 + \left(0.178\Omega_y\right)^2}}, & \theta_j < 0.16\pi \ (horizontal\ logic) \\ \sqrt{\dfrac{\left(\left(L_f - B_M\right)\cos\alpha_{AP}\right)^2}{1 + \left(0.178\Omega_y\right)^2}}, & 0.16\pi \leq \theta_j \leq \dfrac{\pi}{3} \ (45^\circ\ inclination\ logic) \end{cases} \quad (104)$$

To model scenarios where the Johnson model predicts the impact of crosswinds giving rise to flames that bend back on themselves, X_2 is assigned a negative value if the value of X, calculated from equation (6) is less than the Johnson model's predicted frustum lift off distance, determined from equation (22).

4.10 Modelling of radiation impact on planar observers

Planar observers represent objects for which radiation impact may only be experienced on an exposed surface i.e., with a given orientation and inclination in space, relative to the radiation source (e.g., distinction between radiation received on a front facing surface as against its back [covered] end, radiation measurement readings on narrow-angle radiometers). With point observers however, there is no restriction in terms of observer orientation or inclination on received radiation.

The Miller (2017) model conservatively models radiation impact from simulated multi-point source jet flames to point observers only.

The radiation intensity, I [W/m^2], received by an observer is a product of the flame emissive power, Q_{rad} [W], and an effective geometric intensity I' with dimensions [/m^2].

$$I = Q_{rad} I' \quad (105)$$

The geometric intensity (I') for radiation received by point observers from radiating point sources along the flame centreline (L_f) may be expressed as an integral given by:

$$I' = \int_0^{L_f} \frac{\tau f(l)}{max(4\pi D^2, 1)} dl \quad (106)$$

The M-MPS model has been extended to support radiation impact to planar observers as well, with equation (127) re-written as:

$$I' = \int_0^{L_f} \frac{\tau f(l) cos(\beta_2)}{max(4\pi D^2, 1)} dl \quad (107)$$

Where:

$\underline{D}$	=	vector from a radiating point P along the flame centreline (L_f) to the observer, O ($\underline{o} - \underline{p}$)
β_2	=	angle between the observer plane normal ($\underline{n}_o$) and $-\underline{D}$
τ	=	atmospheric transmissivity, the fraction of radiation not absorbed by the atmosphere
f(l)	=	weighting factor representing the proportion of energy being emitted at different positions along the flame length (see section 4.7)

4.11 Application of numerical integrators for radiation effect modelling

Miller (2017) models radiation emitted along the flame centreline in terms of a weighting factor f(l), representing the proportion of combustion energy multiplied by a fixed fraction of heat radiated at different positions along the flame length. The model employs a discrete approach in integrating the combined radiation impact from all point sources modelled

along the flame centreline length (L_f). The (n) radiating sources are evenly distributed along the flame centreline with the radiating heat weighting factor at a point (*i*), i.e., $f(l_i)$ given by:

$$f(l_i) = J(l_i)K + G \quad (108)$$

Where:

$$G = \frac{1}{\sum_{i=1}^{\frac{2n}{3}-1} i + \frac{1}{2}\left(\frac{2n^2}{9} + n + 1\right)} \quad (109)$$

$$K = \frac{3G}{2}\left(\frac{2n}{3} - 1\right) \quad (110)$$

$$J(l_i) = \begin{cases} \frac{2}{3}\left(\frac{i-1}{\left(\frac{2n}{3}-1\right)}\right), & i \leq \frac{2n}{3} \\ \frac{2}{3} - 2\left(\frac{i}{n} - \frac{2}{3}\right), & \frac{2n}{3} < i \leq n \end{cases} \quad (111)$$

The geometric intensity (I') for radiation received by point and planar observers, as calculated using the discrete approach, is given, respectively as:

For point observers:

$$I' = \sum_{i=1}^{n} \frac{\tau f(l_i)}{max(4\pi D_i^2, 1)} \quad (112)$$

While, for planar observers:

$$I' = \sum_{i=1}^{n} \frac{\tau f(l_i) cos(\beta_2)}{max(4\pi D_i^2, 1)} \quad (113)$$

Note that $f(l_i)$ is maximum at the radiant centre of the flame, i.e., $2L_f/3$ away from the release source and a minimum at each end (Miller, 2017).

The M-MPS model has been extended to support the use of numerical integrators in evaluating radiation impact at observer locations. The radiating heat weighting factor at a normalized length $f(l_{norm})$ along the flame centreline is given by[11]:

$$f(l_{norm}) = 3(J(l_{norm}) + G) \quad (114)$$

Where:

$$J(l_{norm}) = \begin{cases} \frac{l_f}{L_f}, & l_f \leq \frac{2L_f}{3} \\ \frac{2}{3} - 2\left(\frac{l_f}{L_f} - \frac{2}{3}\right), & \frac{2L_f}{3} < l_f \leq L_f \end{cases} \quad (115)$$

l_f is any distance along the flame centreline measured from the release point, while the normalized length, l_{norm}, is given by l_f/L_f. The geometric intensity (I') for radiation received by point and planar observers, as calculated by numerical integrators, is given, respectively as:

For point observers:

[11] NOTE: The expression for $f(l_{norm})$ includes the minimum radiative fraction term "G" to ensure that the integral applies a finite radiative fraction at the flame ends. By default, G is calculated with n=30, in alignment with Miller (2017) and AP Flame. G tends to zero as n tends to infinity.

$$I' = \int_0^1 \frac{\tau f(l_{norm})}{max(4\pi D^2, 1)} d(l_{norm}) \quad (116)$$

While, for planar observers:

$$I' = \int_0^1 \frac{\tau f(l_{norm}) cos(\beta_2)}{max(4\pi D^2, 1)} d(l_{norm}) \quad (117)$$

4.12 Finite flame lift-off distance and height relative to release location

As indicated in section 4.5, the Miller (2017) model assumes jet flames to burn very close to source, i.e., with zero flame lift off distance (B). This assumption is somewhat tenable for hydrogen[12], given its high laminar burning velocity, wide flammability limits, hence, propensity to burn (high combustion reactivity/potential). For less reactive materials, e.g., hydrocarbons, field/experimental evidence on jet flames[3,4], suggest a finite (flame lift-off) distance exists between the release source and onset of visible combustion.

As such, the M-MPS model has been extended to support the modelling of a finite flame lift-off distance (B) given by:

$$B = 0.2 B_M \quad (118)$$

4.13 Application of the HyRAM radiative fraction correlation

The M-MPS model has been extended to support the HyRAM[15] flame radiative fraction (F_{AP}) correlation for pure hydrogen releases, i.e., as an alternative to the Miller (2017) model correlations (see equations (91) to (96).

The HyRAM flame radiative fraction correlation is given by:

$$F_{AP} = 9.45 \times 10^{-9} \left(t_f a_p T_1^4\right)^{0.47} \quad (119)$$

Where:

t_f	=	Flame residence time [ms]
a_p	=	Planck-mean absorption coefficient for an optically thin flame (0.23 for hydrogen)

The flame residence time (t_f) is given by:

$$t_f = \frac{\pi \rho_f W_f^2 L_f W_{st}}{12m} \quad (120)$$

Where the flame characteristic width (W_f) and flame density (ρ_f) are given by:

$$W_f = 0.17 L_f \quad (121)$$

$$\rho_f = \frac{P_o W_p}{R_g T_1} \quad (122)$$

[12] Review of infra-red/thermal imaging pictures taken from field tests involving jet flames from high pressure hydrogen releases seem to indicate the existence of an unburnt core of the flame near the release point (i.e., finite lift-off distance). This observation is corroborated by CFD (KFX) simulations of some of these field tests: where predicted results show very good agreement when compared against observed flame characteristics. These CFD (KFX) simulations indicate that the unburnt core is due to supersonic jet velocity from these high-pressure releases preventing flame propagation back to the release point (i.e., finite post-expansion distances and/or insufficient air entrainment close to the release point to support combustion).

4.14 The flame (centreline) co-ordinates

The flame simulated by the M-MPS model is defined by three points along the flame centreline (L_f), i.e., the x, y and z-axis co-ordinates of the flare tip/lift-off distance, end positions of the flame momentum section length (B_M) and flame tip (R_L). The M-MPS flame centreline co-ordinates (x_0, y_0, z_0), (x_1, y_1, z_1) and (x_2, y_2, z_2), are given by:

$$(x_0, y_0, z_0) = \left(B\left|cos\,\theta_j\right|, 0, B\,sin\,\theta_j + z_{Elev}\right) \qquad 0 \le \theta_j \le 90 \qquad \textbf{(123)}$$

$$(x_1, y_1, z_1) = \left(B_M\left|cos\,\theta_j\right|, 0, B_M\,sin\,\theta_j + z_{Elev}\right) \qquad 0 \le \theta_j \le 90 \qquad \textbf{(124)}$$

$$(x_2, y_2, z_2) = \left(x_1 + R_L\,cos\,\lambda\cos\varphi_{flame}, R_L\,cos\,\lambda\sin\varphi_{flame}, z_1 + R_L\,sin\,\lambda\right) \qquad 0 \le \theta_j \le 90;\ 0 \le \theta_{jv} \le 90 \qquad \textbf{(125)}$$

Where:

$$\varphi_{flame} = \begin{cases} tan^{-1}\left(\dfrac{\frac{R_L}{sin\,\theta_{jv}}sin\,\alpha_{AP}\,sin\,\phi}{\frac{R_L}{sin\,\theta_{jv}}\left[sin(\theta_{jv}-\alpha_{AP})\,cos\,\theta_j + sin\,\alpha_{AP}\,cos\,\phi\right]}\right), & vertical\ releases \\ \varphi_{flame}, & non-vertical\ releases \end{cases} \qquad \textbf{(126)}$$

$$\lambda = \begin{cases} sin^{-1}\left(\dfrac{sin\,\theta_j\left(sin(\theta_{jv}-\alpha_{AP,vert})\right)}{sin\,\theta_{jv}}\right), & for\ vertical\ releases \\ \alpha_{AP}, & for\ non-vertical\ releases \end{cases} \qquad \textbf{(127)}$$

5 ADJUSTMENT OF JET FIRE FOR TIME VARYING RELEASES

5.1 Options available

The JFSH model at present uses one flame shape to represent the history of the fire. This is a limitation considering that many releases will have a flame shape that changes significantly with time[13]. Some unhelpful model behaviour has been observed when the default source term assumptions are applied. For instance, stopping the release earlier may give a larger jet fire than with a longer release time because the early stages of the release have a higher release rate. The jet fires modelled may also become misleadingly large because in practice there is a limit to how quickly the released material can burn.

In the product there are four methods for calculating the average discharge rate to represent the time varying behaviour in the linked modelling. These methods affect dispersion, flash fires, explosions and jet fires in different ways. For a full description please see the product help – (hint: search for Time varying releases tab).

Table 1 lists the four options and describes their impact on jet fire modelling[14]:

Table 1 Methods for calculating average rates and impact on jet fire modelling

Method for calculating average rate	Impact on jet fire modelling
Average rates	The discharge rate used will be the average over the time-scale of interest set by the **Jet fire averaging time** in the Jet fire parameters.
Given time	The discharge rate used will be the rate at this particular time or the rate at the end of the release if the time is greater than the release duration.
Average between two times	The discharge rate used will be the average rate between the two times specified. If the release stops before the end of this period then the discharge rate will be averaged up to the point the release stops.

[13] Improve: introduce flames that change more realistically with time. In many ways this will reduce the complexity caused by the model limitations.

[14] Improve: make the choice of jet fire approach more transparent in the product

Method for calculating average rate	Impact on jet fire modelling
Up to 10 rates	The discharge rate used will be the average over the time-scale of interest set by the **Jet fire averaging time** in the Jet fire parameters. This effectively means this option causes the jet fire modelling to behave in the same way as that for 'Average rates'

The 'Average rates' and 'Up to 10 rates' options provide a mechanism for users to specify jet fire modelling to be based on a discharge rate that is different from that used for other consequence modelling (dispersion, flash fires, etc).

The four methods listed above become irrelevant for jet fires if a 'fireball matching method' is enabled. This method is triggered when the options 'model short duration effects for time varying releases' and 'Match fireball duration and mass released' are selected.

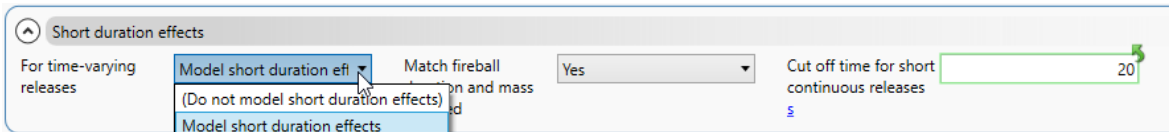

5.2 Fireball matching method

The flow rate in the first 20s can drop quite significantly and if the average is used then the fire size may be somewhat underestimated. Furthermore, if the release is cut off before the end of the averaging period then the average used becomes higher even though intuitively the hazards and risk should reduce if a release is cut off earlier.

To compensate somewhat for this there is a method that uses the matching fireball mass to adjust the fire size.

This causes the linked modelling to calculate a representative fireball mass. This is used to define a maximum mass burning rate for the jet fire flame. This same fire size will then be used even if the release duration reduces or increases.

Using this method the fuel mass rate = (fireball mass)/(fireball duration). The duration used for the jet is then adjusted to compensate. It uses the larger of the fireball duration, release duration and original averaged jet fire duration. It will then cap this value to the 'Cut off time for short duration releases'.

6 ADJUSTMENT OF FLAME SHAPE IN CASE OF GROUND IMPINGEMENT[15]

Depending on the release elevation and release direction, the predicted flame could impinge the ground and penetrate the ground if not modified. In the jet fire models before Phast 8.0, JFSH issues an error message in case the central-line of the predicted jet-fire cone penetrates the ground and a warning if any part of cone penetrates the ground but not by the central-line. Following the validation of liquid/2-phase jet fires as described in the companion validation document, the predicted jet-fire cone is now rotated and/or uplifted in case the cone hits the ground to improve the predictions. However, the shape of the predicted cone is maintained, i.e. frustum widths and length are not changed Figure 7 shows the cases considered for adjustment.

[15] Improve?: Adjustment for flame in case of ground impingement is only applicable to JFSH cone models and not to the M-MPS model.

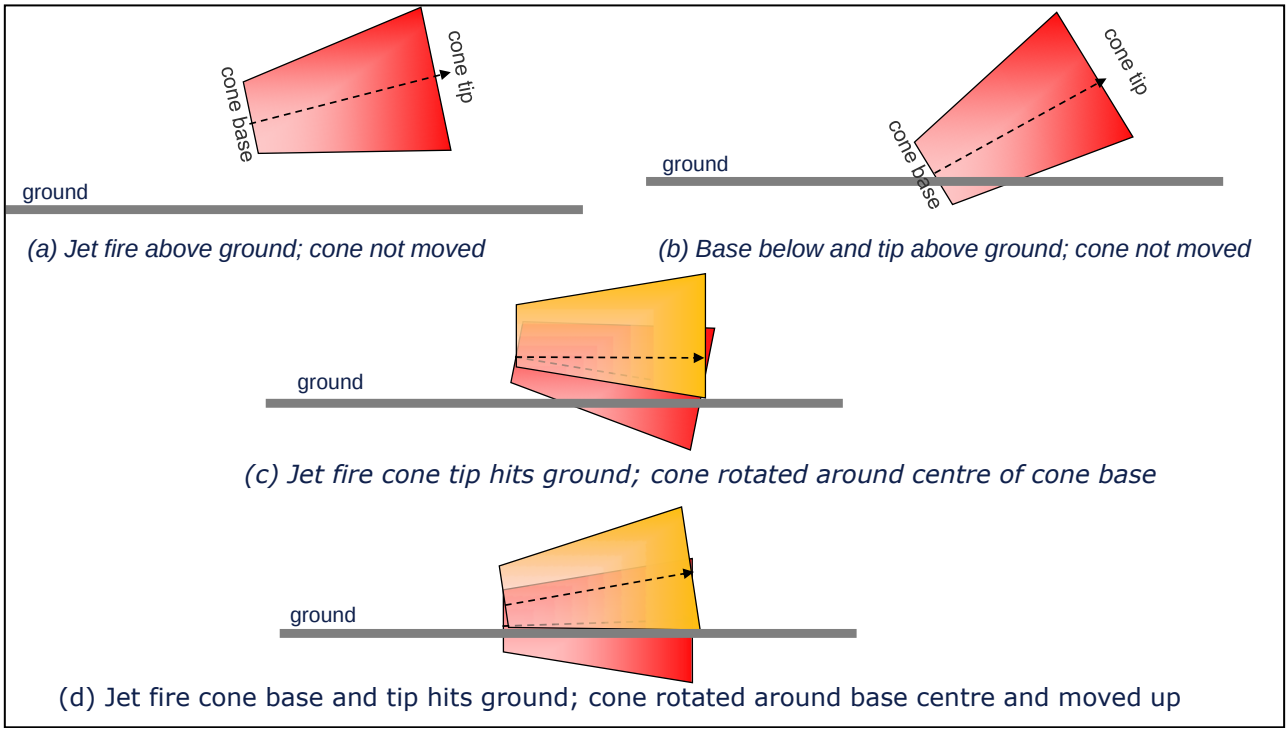

Figure 7 Flame adjustment for flame penetrating the ground

As illustrated in Figure 8, the vertical heights Z_A and Z_B above the ground of the low points of the predicted cone flame can be expressed by

$$Z_A = Z_1 - \left(\frac{W_1}{2}\right)\cos\beta \quad \textbf{(128)}$$

$$Z_B = Z_1 + \left(\frac{W_2}{2}\right)\cos\beta \quad \textbf{(129)}$$

where

Z_1 = Vertical height above the ground of the frustum base centre [m]
β = Angle between central-line of the cone and the horizontal [radians; $-\pi<\beta\leq\pi$]

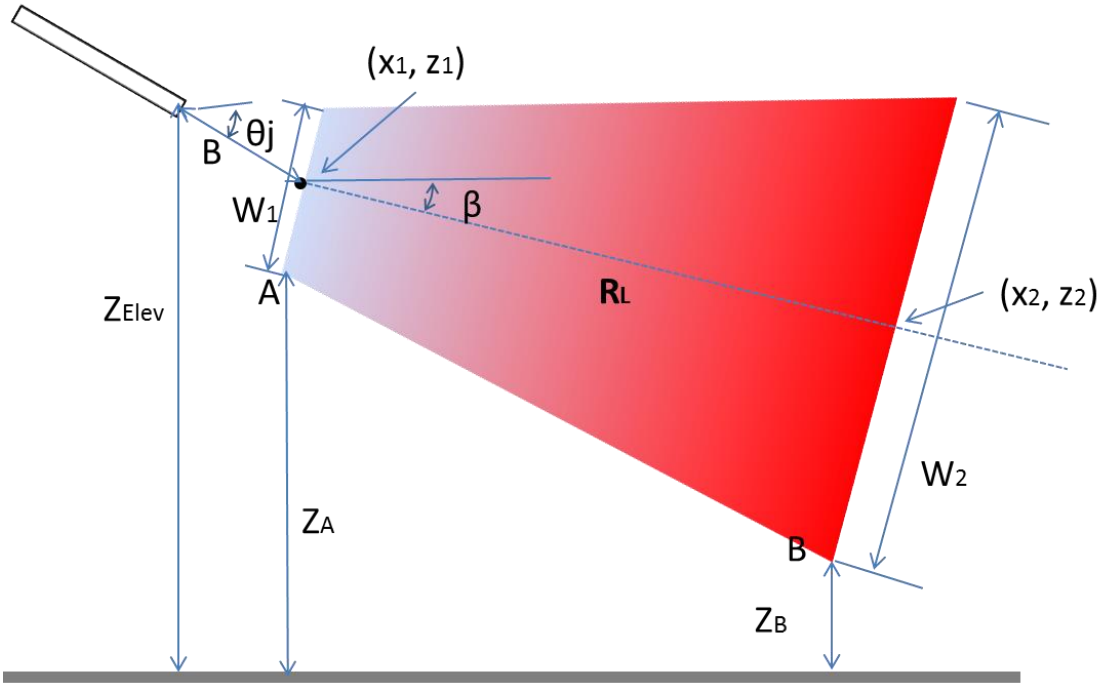

Figure 8 Determining the adjusted flame position

In case the fire cone hits the ground, the new adjusted position of the cone is obtained by adjusting the values of Z_1 and

(a) <u>The predicted flame is above the ground</u>
The predicted flame is fully above the ground, i.e. $Z_A \geqslant i.\& Z_B \geqslant$, and no adjustment is needed.

(b) <u>Predicted cone only penetrates the ground at the base and not at the top</u>
In case the predicted cone penetrates the ground only at base and not at the top, i.e. Z_A <0 & Z_B ≥0, the jet-fire cone is not uplifted to be above the ground because an uplift would make the predicted radiation at the ground level less conservative. Thus no adjustment is applied.

(c) <u>Base of fire cone entirely above ground and tip of fire cone penetrates the ground</u>
In this case, base of the predicted jet-fire cone is above the ground, but the flame top impinges the ground, i.e. Z_A *i.&* Z_B <0. The location of the centre of cone base is fixed, and the cone is rotated around the base centre until point B is on the ground, i.e. Z_1 is kept unchanged, and the adjusted position is obtained by solving the equation (63) for β when Z_B is set to zero.

(d) <u>Both base and top of the predicted flame penetrate the ground</u>
If both base and top of the predicted cone penetrate the ground, i.e. Z_A *<0 &* Z_B <0, the cone is then shifted upwards and rotated until points A & B are on the ground. The adjusted position of the cone is determined by first setting $Z_A = 0$, $Z_B = 0$, and subsequently solving the equations (62) & (63) for new Z_1 and β.

There are some validation results presented in the companion validation document.

7 FUTURE DEVELOPMENTS

The following are recommendations for further work on the present jet fire model.

- Further validation vs field tests as data becomes available
- Validation vs Spadeadam liquid hydrogen tests
- Adapt some aspects of the Sandia model and see if this improves validation (curved flame, emissive power correlation)
- Adjust the Miller model radiation calculations to avoid overprediction along the flame axis

NOMENCLATURE

A	total surface area of the flame (conical frustum) [m^2]
B	frustum lift-off height/distance [m]
B_M	momentum dominated flame length [m]
d_o	orifice or discharge diameter [m]
D_s	combustion or effective source diameter [m]
F	Mach number of non-choked discharging fluid at stagnation temperature and ambient pressure [-]
F_{AP}	Flame radiant heat fraction along the flame centreline [-]
F_s	fraction of heat radiated from the surface of the flame [-]
g	gravitational acceleration [m/s^2]
H_{COMB}	heat of combustion of the fuel mixture [J/kg]
L_B	flame length measured from tip of flame to centre of exit plane [m]
L_{B0}	flame length in still air [m]
L_f	flame centreline length [m]
m	mass flow rate [kg/s]
M_d	mass release rates from discharge calculation [kg/s]
M_j	Mach number of the expanded jet [-]
M_W	fluid's molecular weight [g/mol]
M_{Wkg}	fluid's kilogram molecular weight [kg/mol]
P_c	static or choke pressure at the discharge plane [N/m^2]
P_o	atmospheric pressure [N/m^2]
Q_{rad}	total heat radiating (flame emissive power) from the flame along the flame centreline [W]
r_j	expanded radius of the escaping fluid [m]
$r_{jetmass}$	mass modification factor for jet fire calculation
R	ratio of wind speed to post-expansion jet velocity [-]
R_g	gas constant [8.314 J/mol/K]
R_L	flame frustum length [m]
t_j	durations of the release rate [s]
t_{jet}	jet fire average time (set under jet fire parameters) [s]
T_{Air}	atmospheric temperature [K]

T_c	temperature at discharge plane during choked discharge [K]
T_j	post-expansion discharge temperature [K]
T_s	stagnation temperature [K]
T_1	adiabatic combustion temperature [K]
U_w	wind speed [m/s]
v_j	post-expansion velocity of fluid [m/s]
W_{st}	Mass fraction of fuel in a stoichiometric mixture with air [-]
W_{Air}	Molecular weight of air [g/mol]
W_p	Mean product molecular weight [g/mol]
$W_{surface}$	Surface emissive power of flame [W/m^2]
W_1	width of frustum base [m]
W_2	width of frustum tip [m]
x_1	horizontal distance of the frustum base from the virtual origin along the vertical plane cutting the flame into symmetrical halves [m]
x_2	horizontal distance of the frustum tip from the virtual origin along the vertical plane cutting the flame into symmetrical halves [m]
z_{Elev}	elevation of the release point (e.g., flare tip) from the horizontal plane [m]
z_1	vertical distance of the frustum base from the virtual origin along the vertical plane cutting the flame into symmetrical halves [m]
z_2	vertical distance of the frustum tip from the virtual origin along the vertical plane cutting the flame into symmetrical halves [m]

Greek letters

α	angle between hole axis and flame axis [degrees]
β	constant in Becker and Liang's[10] flame length correlation
ϕ	angle between the wind vector and the projection of the release axis on the horizontal plane [degrees]
ϕ_{flame}	angle between the vertical planes cutting the release source and jet flame respectively into symmetrical halves [degrees]
γ_g	ratio of specific heats [-]
$\eta_{rainout}^{i}$	rainout mass fraction for segment i (kg/kg)
ϑ	inclination of the frustum base to the horizontal plane [degrees]
θ_j	angle between hole axis and the horizontal in the vertical plane [degrees]
θ_{jv}	angle between hole axis and wind vector in the plane containing the hole axis, flame axis, and wind vector [degrees]
ρ_{amb}	density of air at ambient conditions [kg/m^3]

ρ_j	density of expanded fluid jet [kg/m^3]
$\rho_{T_{SatVap}}$	Fuel's saturated vapour density at ambient pressure [kg/m^3]
$\xi(D_s)$	Richardson number based on D_s (i.e., source diameter) [-]
$\xi(L_{B0})$	Richardson number based on flame length in still air [-]

REFERENCES

1 Van den Bosch C. J. H., and Wetterings R. A. P. M. (Eds), “Methods for the calculation of physical effects ‘Yellow Book’ CPR 14E (Part 2)”, 3rd ed., Sdu Uitgevers, The Hague, pp 6.17-6.138, (1997)

2 American Petroleum Institute, “Guide for pressure relieving and depressurising systems”, API RP 521, 2nd ed., (September 1982)

3 Chamberlain, G. A., “Developments in design methods for predicting thermal radiation from flares”, Chem. Eng. Res. Des., Vol. 65, pp 299-309, (July 1987)

4 Johnson, A. D., Brightwell, H. M., and Carsley, A. J., “A model for predicting the thermal radiation hazard from large scale horizontally released natural gas jet fires,” Trans. IChemE., Vol. 72, Part B, pp 157-166, (1994)

5 Miller, D., “New model for predicting thermal radiation from flares and high pressure jet fires for Hydrogen and Syngas”, Process Safety Progress, Vol. 36, No. 3, pp 237 – 251, (September 2017)

6 Harper, M., “Continuous and Instantaneous Discharge Models (DISC)”, DNV (July 2002)

7 Holt, A., Topalis, P., Witlox, H. W. M., Clements, F., and Harper, M., “Atmospheric Expansion Model (ATEX),” DNV (July 2002).

8 Cook, J., Bahrami, Z., Whitehouse, R. J., “A comprehensive program for calculation of flame radiation levels”, J. Loss Prev. Process Ind., 3, pp 150-155, (1990)

9 Kalghatgi, G. T., “Lift-off heights and visible flame lengths of vertical turbulent jet diffusion flames in still air”, Combustion Science and Technology, 41, Nos 1-2, pp 17-29, (1984)

10 Becker, H. A. and Liang, D., “Visible length of vertical free turbulent diffusion flames”, Combustion and Flame, 32, pp 115-137, (1978)

11 TECHNICA, “Flare theory manual”, C321.8/138/2, pp 12, (July 1989)

12 Chamberlain, G. A., Private Communication - email 27 September 2011 (2011)

[13] Bennett, J. F., Cowley, L. T., Davenport, J. N., and Rowson, J. J., “Large scale natural gas and LPG jet fires final report to the CEC”, TNER 91.022, (1991)

14 Prothero, A., “EP/Technica Study- Near Platform Releases”, ctt1apr/epcond, Shell Research Ltd, Thornton Research Centre, Chester, pp 1 (23rd May, 1989)

15 Ehrhart, B. D., Hecht, E. S., “Hydrogen risk assessment models (HyRAM), version 3.0 technical reference manual”, Sandia report, SAND2020-10600, Sandia National Laboratories, Albuquerque, New Mexico (September 2020)

About DNV

We are the independent expert in risk management and quality assurance. Driven by our purpose, to safeguard life, property and the environment, we empower our customers and their stakeholders with facts and reliable insights so that critical decisions can be made with confidence. As a trusted voice for many of the world's most successful organizations, we use our knowledge to advance safety and performance, set industry benchmarks, and inspire and invent solutions to tackle global transformations.

Digital Solutions

DNV is a world-leading provider of digital solutions and software applications with focus on the energy, maritime and healthcare markets. Our solutions are used worldwide to manage risk and performance for wind turbines, electric grids, pipelines, processing plants, offshore structures, ships, and more. Supported by our domain knowledge and Veracity assurance platform, we enable companies to digitize and manage business critical activities in a sustainable, cost-efficient, safe and secure way.